



HHS Public Access

Author manuscript

Free Radic Biol Med. Author manuscript; available in PMC 2022 February 20.

Published in final edited form as:

Free Radic Biol Med. 2021 February 20; 164: 271–284. doi:10.1016/j.freeradbiomed.2021.01.003.

β -carotene oxygenase 2 deficiency-triggered mitochondrial oxidative stress promotes low-grade inflammation and metabolic dysfunction

Lei Wu^{1,*}, Peiran Lu¹, Xin Guo¹, Kun Song², Yi Lyu¹, James Bothwell¹, Jinglong Wu¹, Olivia Hawkins¹, Stephen L. Clarke¹, Edralin A. Lucas¹, Brenda J. Smith¹, Winyoo Chwanadisai¹, Steve D Hartson³, Jerry W. Ritchey⁴, Weiqun Wang⁵, Denis M. Medeiros⁶, Shitao Li², Dingbo Lin^{1,**}

¹ Department of Nutritional Sciences, Oklahoma State University, Stillwater, OK 74078, USA

² Department of Microbiology and Immunology, Tulane University, New Orleans, LA 70112

³ Department of Biochemistry and Molecular Biology, Oklahoma State University, Stillwater, OK 74078, USA

⁴ Department of Veterinary Pathobiology, Oklahoma State University, Stillwater, OK 74078, USA

⁵ Department of Food, Nutrition, Dietetics, and Health, Kansas State University, Manhattan, KS 66506, USA

⁶ Department of Molecular Biology and Biochemistry, University of Missouri-Kansas City, Kansas City, MO 64110, USA

Abstract

Low-grade inflammation is a critical pathological factor contributing to the development of metabolic disorders. β -carotene oxygenase 2 (BCO2) was initially identified as an enzyme catalyzing carotenoids in the inner mitochondrial membrane. Mutations in *BCO2* are associated with inflammation and metabolic disorders in humans, yet the underlying mechanisms remain unknown. Here, we used loss-of-function approaches in mice and cell culture models to

**Corresponding author: Dingbo Lin, Ph.D., Department of Nutritional Sciences, Oklahoma State University, Stillwater, OK 74078, USA, Phone: 1-405-744-5215, Fax: 1-405-744-1357, dingbo.lin@okstate.edu.

*Current address: Key Laboratory of Animal Physiology and Biochemistry, Ministry of Agriculture and Rural Affairs, College of Veterinary Medicine; MOE Joint International Research Laboratory of Animal Health & Food Safety, Nanjing Agricultural University, Nanjing 210095, Jiangsu, China

Statement of Author Contributions

LW, SDH, JWR, DMM, WW, SLC, EAL, BJS, WC, SL, and DL designed the study; LW, XG, JB, KS, PL, OH, YL, and DL conducted the research; XG, LW, SDH, JWR, WC, and DL analyzed the data; XG, DMM, WW, SLC, BJS, EAL, WC, JWR, SL, and DL wrote and revised the manuscript. All authors read and approved the final manuscript. The corresponding author verifies that all individuals who made contributions to this study have been included as authors.

Competing interests

No competing interests declared

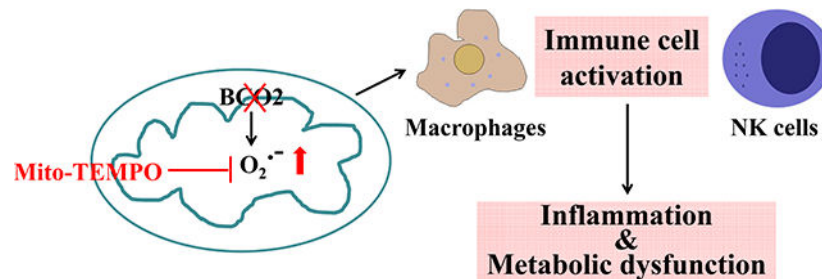
Data Statement

Raw data are available upon request

Publisher's Disclaimer: This is a PDF file of an unedited manuscript that has been accepted for publication. As a service to our customers we are providing this early version of the manuscript. The manuscript will undergo copyediting, typesetting, and review of the resulting proof before it is published in its final form. Please note that during the production process errors may be discovered which could affect the content, and all legal disclaimers that apply to the journal pertain.

investigate the role of BCO2 in inflammation and metabolic dysfunction. We demonstrated decreases in *BCO2* mRNA and protein levels and suppression of mitochondrial respiratory complex I proteins and mitochondrial superoxide dismutase levels in the liver of type 2 diabetic human subjects. Deficiency of BCO2 caused disruption of assembly of the mitochondrial respiratory supercomplexes, such as supercomplex III₂+IV in mice, and overproduction of superoxide radicals in primary mouse embryonic fibroblasts. Further, deficiency of BCO2 increased protein carbonylation and populations of natural killer cells and M1 macrophages, and decreased populations of T cells, including CD4⁺ and/or CD8⁺ in the bone marrow and white adipose tissues. Elevation of plasma inflammatory cytokines and adipose tissue hypertrophy and inflammation were also characterized in BCO2 deficient mice. Moreover, BCO2 deficient mice were more susceptible to high-fat diet-induced obesity and hyperglycemia. Double knockout of *BCO2* and leptin receptor genes caused a significantly greater elevation of the fasting blood glucose level in mice at 4 weeks of age, compared to the age- and sex-matched leptin receptor knockout. Finally, administration of Mito-TEMPO, a mitochondrial specific antioxidant attenuated systemic low-grade inflammation induced by BCO2 deficiency. Collectively, these findings suggest that BCO2 is essential for mitochondrial respiration and metabolic homeostasis in mammals. Loss or decreased expression of BCO2 leads to mitochondrial oxidative stress, low-grade inflammation, and the subsequent development of metabolic disorders.

Graphical Abstract



Keywords

Diabetes; human; macrophage; mitochondrial respiratory supercomplex assembly; natural killer cell; superoxide

Introduction

Low-grade inflammation, also called chronic inflammation, is featured by immune cell activation and moderate increases in inflammatory markers present in the central circulation and tissues [1]. It often does not have clinical symptoms, particularly at the early stage of the disease process. However, prolonged low-grade inflammation can contribute to the development of several metabolic disorders, including but not limited to insulin resistance, hyperglycemia, dyslipidemia, and adipocyte hypertrophy and obesity [2–4]. These metabolic disruption caused by low-grade inflammation has become significant health issues in both developed and under-developed countries. Therefore, precisely understanding the causes and

effects of low-grade inflammation is critical for the development of strategies in the treatment and/or prevention of low-grade inflammation and its relevant metabolic diseases.

Low-grade inflammation can be caused by heritable genetic factors and be triggered by environmental factors, such as lifestyle, diet, and exposure to environmental contaminants [5–7]. Numerous bodies of evidence show that the mitochondria are not only the powerhouse of the cell but also function as signaling organelles in the immune response and low-grade inflammation [8–9]. Accumulation of mitochondria-derived superoxide radicals, e.g., mitochondrial oxidative stress, causes damages to biological molecules, such as DNA, RNA, lipids, and proteins inside and outside of mitochondria [10–12]. Consequently, mitochondrial dysfunction and associated oxidative stress exhibit an essential role in immune cell activation and immune responses, resulting in low-grade inflammation.

β -carotene oxygenase 2 (BCO2) is a carotenoid cleavage enzyme located to the inner mitochondrial membrane (IMM) [13]. Mutations and deletion of BCO2 induce carotenoid accumulation in laboratory mice and other animal models when fed a carotenoid diet [13–15]. Expression of *BCO2* transcripts is developmentally regulated for sexual dichromatism and carotenoid ornamentation (or coloration) in peripheral tissues in birds, poultry, and other domestic avian species [16–19]. Carotenoid-based coloration could be controlled through switches in the regulation of enzymatic activity or *BCO2* expression levels [19]. The human *BCO2* gene expresses five protein splice variants. Interestingly, published data suggest that BCO2 might be enzymatically inactive in the retina of humans, where macular carotenoids are preferentially deposited [20–22]. Observational clinical research also confirmed that BCO2 deficiency and mutations are associated with low-grade inflammation and metabolic disorders in human subjects [20, 23–25]. We recently reported that loss of BCO2 is related to impaired mitochondrial respiration and cellular oxidative stress in mouse models [26, 27]. Therefore, there is a need to elucidate additional roles for BCO2 beyond carotenoid metabolism and determine if BCO2 can regulate mitochondrial redox homeostasis in mammals.

In this current study, we hypothesized that BCO2 is essential to mitochondrial redox balance by regulating mitochondrial respiratory supercomplex assembly. Deficiency of BCO2 leads to mitochondrial oxidative stress and consequent metabolic dysfunction. To validate this hypothesis, we first examined whether BCO2 deficiency was associated with mitochondrial respiration and oxidative stress in the liver of type 2 diabetic human subjects. Next, we determined the effect of BCO2 on mitochondrial respiratory complex assembly, oxidative stress, low-grade inflammation, and metabolic dysfunction in BCO2 knockout (KO) mice and overexpression cell culture models. Further, we characterize the susceptibility of BCO2 KO mice to obesity and diabetes in models of high-fat induced obesity and/or BCO2 and leptin receptor (LepR) double knockout mice. Finally, we offset the low-grade inflammation in BCO2 KO mice by systemic application of Mito-TEMPO, a mitochondrial specific antioxidant, which demonstrated the link between mitochondrial oxidative stress and inflammation in BCO2 deficiency.

Materials and Methods

Human liver specimen and BCO2 expression assessments

Liver tissue specimens were purchased from the Sekisui-XenoTech Biobank (Kansas City, KS, USA). In total, we obtained 3 specimens of healthy controls (C1, C2, C3) and 3 specimens of type 2 diabetic patients (D1, D2, D3). Tissues were divided and stored in RNAlater or sterile PBS at -80°C for long-term storage. The patients' detailed information was provided in Supplemental Table S1. Hepatic *BCO2* mRNA expression was assessed by real-time PCR. Hepatic protein expression of BCO2 and other mitochondrial proteins was determined by immunoblotting, as described below.

Mouse strains, husbandry, BCO2 and db/db double knockout, and high-fat diet treatments

Two strains of whole-body BCO2 knockout mice (homozygous) in either 129S6 (WT) or C57BL/6J (WT(B6)) backgrounds (e.g., KO and KO(B6), respectively) were maintained in the Laboratory Animal Research Facility at Oklahoma State University (OSU, Stillwater, OK, USA). The colonies were kept on a daily 12-hour light/dark cycle and fed a standard chow diet (AIN 93M) and water *ad libitum* from the Research Diets, Inc (New Brunswick, NJ, USA). All animal protocols and procedures were approved by the Institutional Animal Care and Use Committee (IACUC) at OSU (the breeding colony ACUP# HS-13-4 and the research ACUP# HS-14-4).

BCO2 KO(B6) homozygous and db/db heterozygous (Het) mice were backcrossed to obtain double knockout homozygous mice, or KO(B6)/db/db, with deficiencies of *BCO2* and *LepR* genes [28]. Mice from the following 6 groups at 4 weeks of age were used for fasting blood glucose test and other assessments, WT(B6), KO(B6), KO(B6)/dbHet, KO(B6)Het/dbHet, db/db, and KO(B6)/db/db, n=6–12.

For high-fat (HF) dietary treatments, 6-week old male KO and WT mice were fed a low-fat (LF, 10 kCal % fat, 17 kCal % sucrose) or HF diet (45 kCal % fat, 17 kCal % sucrose) *ad libitum* for 28 weeks, totaling four experimental groups (n=12), as WT-LF, KO-LF, WT-HF, and KO-HF. These diets were purchased from Research Diets, Inc. (catalog #s: D12450H (LF) and D12451 (HF)).

Mouse embryonic fibroblast (MEF) cell isolation and mitochondrial superoxide detection by MitoSOX labeling

MEF cells were isolated from mouse embryonic tissue at E10.5–13 of WT and KO mice (homozygous) as described elsewhere [29]. Primary MEFs were cultured in DMEM (with 4.5 g/L glucose) with 10 % fetal bovine serum (FBS) under 5 % CO_2 at 37°C . Mitochondrial superoxide radicals were measured in primary MEFs at passage 4 using MitoSOX (1.5 $\mu\text{mol/L}$) (catalog # M36008, Molecular Probes, Inc., Eugene, OR, USA). The Mito-Tracker solution at 0.4 $\mu\text{mol/L}$ (catalog # MP 7514, Invitrogen, Inc., Carlsbad, CA, USA) was applied to label mitochondria [30]. 4',6-diamidino-2-phenylindole (DAPI) staining was used to determine the number of nuclei. Images were acquired by Keyence BZ-X800E All-in-One fluorescence microscope. MitoSOX signals were quantified via the ImageJ software (NIH, USA), and normalized to Mito-Tracker signals.

Glucose tolerance tests

Intraperitoneal glucose tolerance test (GTT) was performed at 6-week-old male mice of WT and KO (n=6). Mice were fasted for 6 h prior to injection of a 20% glucose solution (2 g glucose/kg body weight). Blood glucose was measured from the tail vein before and after the glucose injection (at 0, 15, 30, 60, and 120 min) using a ReliOn glucometer.

Mito-TEMPO administration in mice

Mito-TEMPO (catalog # SML0737, Sigma-Aldrich, Inc, St Louis, MO, USA) was dissolved in sterile PBS (pharmaceutical grade) to make a stock concentration of 1 mg/mL. Six-week-old male KO mice received intraperitoneal (i.p.) injections of Mito-TEMPO (3.5 mg/kg BW/day, KO-Tempo) or sterile PBS (KO-PBS) for 7 consecutive days [32]. Age- and gender-matched WT mice were injected intraperitoneally with sterile PBS as control (WT-PBS). GTT was performed in mice on day 6 of the Mito-TEMPO administration. At the end of the treatment, mice were euthanized after 3 h fasting. Blood was drawn, and obtained plasma solutions were used for assessment of lipid parameters and cytokines. The liver and skeletal muscles were used for mitochondrial isolation and total protein extraction, as previously described [26]. The bone marrow was also collected for flow cytometry as described below.

Necropsy, blood collection, tissue harvest, histology, and global metabolomics analysis

All mice were euthanized using ketamine/xylazine (0.006–0.01 mL/g BW) after 3 h fasting. Blood was drawn into the EDTA-coated tube and centrifuged to obtain plasma for measuring lipid parameters and cytokines. Liver, adipose (abdominal fat), and gastrocnemius tissues were carefully dissected to avoid contamination of surrounding tissues. Tissue samples for protein extraction were frozen in liquid nitrogen and stored under –80 C until use. For the histology study, pieces of adipose tissue were fixed into 10% neutral buffered formalin. Embedding, sectioning, and hematoxylin & eosin (HE) staining were performed in the Oklahoma Animal Disease Diagnostic Laboratory. For cell size measurements, a minimum of 6 images was taken per mouse (n=5). Adiposoft software was used to measure the size of adipocyte cells [33]. The distribution of cell size was analyzed as a percentage of total counted cells.

Fresh liver (~50 mg liver tissues) was used for global metabolomics profiling assay, conducted by Metabolon, Inc. (Durham, NC, USA) as described previously [34]. Metabolite samples were prepared using the automated MicroLab STAR® system (Hamilton Company, Allston, MA, USA). A recovery standard was added prior to the first step in the extraction process for QC purposes. To remove protein, to dissociate small molecules bound to protein or trapped in the precipitated protein matrix, and to recover chemically diverse metabolites, proteins were precipitated with methanol under vigorous shaking for 2 min (GenoGrinder 2000, Glen Mills Inc., Clifton, NJ, USA) followed by centrifugation. The resulting extracts were divided into two fractions: one for analysis by ultrahigh performance liquid chromatography-tandem mass spectroscopy (UPLC-MS/MS) and gas chromatography-mass spectroscopy (GC-MS). Samples were placed briefly on a TurboVap® (Zymark) to remove the organic solvent. The UPLC-MS/MS platform was based on a Waters ACQUITY UPLC and a Thermo Scientific Q-Exactive high resolution/accurate mass spectrometer interfaced with a heated electrospray ionization (HESI-II) source and Orbitrap mass analyzer operated

at 35,000 mass resolution. One aliquot was analyzed using a column of Waters UPLC BEH C18 (2.1×100 mm, 1.7 μm). Extracts reconstituted in acidic conditions were gradient eluted from a C18 column using water and methanol containing 0.1% formic acid. The samples destined for analysis by GC-MS were dried under vacuum for a minimum of 18 h prior to being derivatized under dried nitrogen using bistrimethyl-silyltrifluoroacetamide. Derivatized samples were separated on a 5% diphenyl / 95% dimethyl polysiloxane fused silica column (20 m x 0.18 mm ID; 0.18 μm film thickness) with helium as the carrier gas and a temperature ramp from 60 °C to 340°C in a 17.5 min period. Samples were analyzed on a Thermo-Finnigan Trace DSQ fast-scanning single-quadrupole mass spectrometer using electron impact ionization (EI) and operated at unit mass resolving power. Raw data were extracted, peak-identified and QC processed using Metabolon's hardware and software. Compounds were identified by comparison to library entries of purified standards or recurrent unknown entities. Metabolon maintains a library based on authenticated standards that contain the retention time/index (RI), mass to charge ratio (m/z), and chromatographic data (including MS/MS spectral data) on all molecules present in the library. Furthermore, biochemical identifications are based on three criteria: retention index within a narrow RI window of the proposed identification, accurate mass match to the library \pm 0.005 amu, and the MS/MS forward and reverse scores between the experimental data and authentic standards. Contents of 1,3-dipalmitoylglycerol (1,3-DPG), 1,2-dipalmitoylglycerol (1,2-DPG), squalene, and 3-hydroxy-3-methylglutarate (HMG) were analyzed by two-tailed Student's t-test, $n=6$.

Mitochondrial respiratory supercomplex formation by Blue Native PAGE (BN-PAGE) and immunoblotting

Hepatic mitochondrial proteins were isolated from fresh liver tissues and solubilized with 1 % digitonin (Sigma, St Louis, MO) as previously described [35, 36]. Digitonin-solubilized mitochondrial proteins were subjected to Blue Native (BN)-PAGE followed by immunoblotting [26]. BN-PAGE gradient gels (3–12%) were purchased from Novex (catalog # BN1001BOX, Life Technologies, Carlsbad, CA, USA). Antibodies against proteins of individual mitochondrial complexes and/or related supercomplexes (SCs) were: NADH: ubiquinone oxidoreductase subunit B6 (NDUFB6) (complex I, or CI), ubiquinol-cytochrome reductase core protein II (UQCRC2) (CIII), and mitochondrial encoded cytochrome C oxidase II (MTCO2) (CIV), respectively.

Immune cell isolation and flow cytometry

Immune cells were isolated from adipose tissue and bone marrow (mainly flushed from both femur and tibia) according to modified protocols published elsewhere [37, 38]. For bone marrow immune cell collection, the tibia and femur were carefully removed and cut at the proximal and distal ends. The bone marrow was flushed from tibia and femur using ice-cold, complete media (DMEM supplemented with 0.5% BSA and 10 mmol/L EDTA, pH 7.4). Bone marrow immune cells were separated by centrifugation at $110 \times g$, 5 min, 4 °C. For adipose tissue immune cells, abdominal fat tissues were minced and digested enzymatically with 1 mg/mL type II collagenase (catalog # C6885, Sigma-Aldrich, Inc) for 45 min to 1 hour at 37°C with continuous shaking. Homogenates were triturated numerous times and passed through a 70–100 μm filter. Adipose tissue immune cells were separated by

centrifugation at $650 \times g$, 10 min, 4°C . Subsequently, red blood cells (RBC) were lysed by RBC lysing buffer (catalog # 349202, BD Biosciences, Inc., San Jose, CA, USA) at room temperature for 7 minutes. After lysing, cell numbers were counted, and cell suspensions were diluted accordingly with staining buffer (catalog # 554656, BD Biosciences, INC.).

Fluorochrome-conjugated antibodies and/or their isotype controls were used to ensure the specificity of immunostaining in flow cytometry analysis. The antibodies used in the current study are listed in Supplemental Table S2. Labeled immune cells were analyzed using a BD FACSAria III (BD Bioscience, Heidelberg, Germany), and respective data analysis was performed with BD FACSDiva™ software package. Mouse T cell sub-populations were first gated on lymphocytes ($\text{CD}3\text{e}^{+}$) and then $\text{CD}4^{+}$ T cells, defined as $\text{CD}3\text{e}^{+}\text{CD}4^{+}$, and $\text{CD}8^{+}$ T cells were defined as $\text{CD}3\text{e}^{+}\text{CD}8\text{a}^{+}$. Mouse bone marrow natural killer (NK) cells were defined as $\text{CD}3\text{e}^{-}\text{CD}16/32^{+}\text{CD}56^{+}$ [39]. Mouse bone marrow M1 macrophages were defined as $\text{CD}11\text{c}^{+}\text{TNF-}\alpha^{+}\text{CD}38^{+}$, and M2 macrophages were defined as $\text{Egr}2^{+}\text{CD}206^{+}\text{Arg}1^{+}$ [40]. Bone marrow-derived, mouse adipose NK cells were defined as $\text{CD}3^{-}\text{CD}45^{+}\text{IL}6\text{Ra}^{+}$ [41].

F4/80⁺ cells in adipocyte tissues by immunohistochemistry

Immunohistochemistry staining was performed as described, with some modifications [42]. Briefly, formalin-fixed, paraffin-embedded adipocyte tissue sections (5 μm in thickness) were deparaffinized, rehydrated, and treated with antigen retrieval buffer (0.01 M citrate acid, pH 6.0). Tissue section samples were incubated in PBST (1x PBS with 0.1% Tween 20) containing 1% (v/v) BSA and 22.52 mg/mL glycine for 1 h, at room temperature; and then incubated with antibody against F4/80 conjugated with FITC (1:100 dilution, catalog # MCA497FB, Bio-Rad, Inc.) overnight at 4°C . These samples were then washed with PBST and further counterstained with DAPI (1:4000) for 1 minute at room temperature to visualize the nucleus. Finally, samples were washed with PBST, mounted with FluorSave™ Reagent (Calbiochem, 345789), and examined under a Keyence BZ-X800E All-in-One fluorescence microscope. F4/80⁺ cells (green) were counted and normalized to nuclei as a proxy for total cell number using DAPI staining for quantification using ImageJ software.

Plasma parameters measurements

Plasma lipid and inflammatory markers were measured as previously described [26, 27]. Plasma concentrations of C-reactive protein (CRP), non-esterified fatty acids (NEFA), total cholesterol (CHOL), triglycerides (TG), low-density lipoprotein CHOL (LDL-C), and high-density lipoprotein CHOL (HDL-C) were measured using a BioLis 24i automated analyzer (Carolina Chemistry, NC, USA). The Bio-Plex MAGPIX Multiplex reader and the corresponding kit (catalog # M60009RDPD/MD000000EL, Bio-Rad Laboratories Inc, Hercules, CA, USA) were used for inflammation markers, including tumor necrosis factor- α (TNF- α), monocyte chemoattractant protein-1 (MCP-1), interleukin 6 (IL-6), interleukin 1 beta (IL-1 β), and IL-18, according to the manufacturer's instruction.

Total protein extraction and immunoblotting analysis

Samples from mouse tissues and human liver specimens were homogenized using a TissueRuptor (Qiagen) in the cell lysis buffer containing 20 mM Tris, pH 7.5, 0.5 mM EDTA, 0.5 mM EGTA, 0.5% Triton X-100, and 1% protease/phosphatase inhibitors [26].

After homogenization, lysates were sonicated and centrifuged at $8,000 \times g$, 4°C , 10 minutes. The supernatants were collected and stored at -80°C for future analysis. Protein concentration was estimated by bicinchoninic acid assay (BCA assay, Pierce, Rockford, IL, USA). Equal amounts of total proteins were separated by SDS-PAGE followed by immunoblotting. Protein expression was normalized to loading controls, β -actin, or glyceraldehyde-3-phosphate dehydrogenase (GAPDH). The antibodies used in the current study are listed in Supplemental Table S3.

Total hepatic triglyceride measurement

Triglyceride content was analyzed using the triglyceride colorimetric assay kit (catalog # 10010303, Cayman Chemical Company, Ann Arbor, MI, USA). Briefly, fresh liver samples (250 mg/specimen) were homogenized in cell lysis buffer supplemented with 1% phosphatase/protease inhibitors and centrifuged at $10,000 \times g$, 4°C , 10 minutes. The supernatant solution was transferred into a new tube and stored under -80°C for TG analysis according to the manufacturer's instructions. The final data were normalized by protein concentration.

Detection of protein carbonylation

Protein carbonylation, a form of oxidative damage, was detected using an OxyBlot protein oxidation detection kit (catalog # S7150, EMD Millipore, Temecula, CA, USA) according to the manufacturer's instruction [43]. Protein samples of white adipocyte (WAT) and gastrocnemius muscle (Muscle) tissues were reacted with 2,4-dinitrophenylhydrazine (DNP-hydrazine) to derivatize the carbonyl groups to 2,4-dinitrophenylhydrazone (DNP-hydrazone). The treated samples were separated by SDS-PAGE followed by immunoblotting [26]. Oxidized protein expression was normalized to β -actin, a loading control.

8-hydroxy-2-deoxyguanosine (8-OHdG) immunofluorescence in MEFs

Endogenous oxidative DNA damage was measured by 8-OHdG immunofluorescence in MEFs. Briefly, 80 % confluent primary MEFs at passage 5 were treated with Mito-TEMPO (2 and/or 20 $\mu\text{mol/L}$, 1 h), PBS as a negative control. After treatments, cells were fixed in ice-cold methanol at -20°C for 10 min, followed by 1-h blocking in 5 % FBS and then 12-h incubation with primary anti-8-OHdG antibody (catalog # sc-393871, 1:100, Santa Cruz Biotech, Dallas, TX, USA) at 4°C . Alexa Fluor 488 antisera (catalog # A28175, 1:400, Molecular Probes, Inc., Eugene, OR, USA) were used as a secondary antibody. DAPI staining was applied to visualize nuclei. Images were acquired by Keyence BZ-X800E All-in-One fluorescence microscope. At least 50 cells per group were viewed and imaged. The experiment was replicated once.

RNA extraction and real-time PCR

Relative gene transcriptional expression was determined by real-time PCR as previously described [44]. Total RNA from human liver and mouse WAT were extracted using the standardized Trizol method and quantified by Nano-drop spectrophotometry. cDNA was synthesized using SuperScript II reverse transcriptase (#18064014, Invitrogen) from extracted total RNA. Real-time PCR analysis was performed by using SYBR Green

chemistry (catalog #4472908, ThermoFisher Scientific) on an ABI 7900HT sequence-detection instrument and 2.4 SDS software (Applied Biosystems). The primers used in this current study are listed in Supplemental Table S4. The relative mRNA abundance was calculated by use of the $2^{-\Delta Ct}$ method [44], and normalized to the control group.

Statistical analysis

All values are expressed as means \pm SD. Unpaired two-tailed Student's t-test was used to determine statistical significance between two groups (such as WT and KO). Statistical significance was set at $P < 0.05$ (* $P < 0.05$; ** $P < 0.01$; *** $P < 0.001$). ANOVA was used for the analysis of data from more than two groups. Labeled means without a common letter differ, $P < 0.05$.

Results

Decreased expression of BCO2 mRNA and protein in human diabetic liver

Real-time PCR and immunoblotting results revealed that the expression levels of hepatic *BCO2* mRNA and proteins were significantly decreased in humans with type 2 diabetes, compared to the healthy control subjects (Figures 1A and 1B). We further determined the protein levels of NDUFA9 and NDUFB6, mitochondrial respiratory complex I proteins, and SOD2, a scavenger of mitochondrial superoxide radicals [45]. Similar to the changes in *BCO2* protein, these three protein levels were also decreased in diabetic livers, compared to healthy controls (Fig. 1C–1D). These data might suggest the link of *BCO2* to mitochondrial function in health and diabetes.

Deficiency of BCO2 disrupts mitochondrial respiratory supercomplex assembly and stimulates mitochondrial superoxide production

We recently reported that *BCO2* deletion is associated with the alteration of mitochondrial respiration activities and cellular oxidative stress in mice [26]. Here, we assessed whether *BCO2* is associated with the assembly of SCs in mitochondria in WT and KO mice, using BN-PAGE followed by immunoblotting with the antibodies against NDUFB6 (CI), UQCRC2 (CIII), MTCO2 (CIV), respectively. The deletion of *BCO2* broadly disrupted assembly of SCs, particularly III₂+IV, and possible other SCs as evaluated by changed positions in Figure 2 A–C, for example, I+ III₂+IV, I+ III₂+IV₂, I₂+ III₂+IV₂, and other megacomplexes, which were not well separated due to limited sizes of these BN-PAGE gels used. Next, we examined the production of superoxide radicals in MEFs generated from WT and KO mice by MitoSOX staining (Red), Mito-Tracker labeled mitochondria in green (Figure 2D, Supplemental Figure S1). In *BCO2* KO MEFs, the relative ratio of MitoSOX/Mito-Tracker signals was significantly stronger than that in WT MEFs, indicating elevated superoxide production in KO MEFs.

Deficiency of BCO2 leads to protein carbonylation and systemic low-grade inflammation

Cellular oxidative stress can cause biological macromolecule oxidation, such as proteins, lipids, and nucleotides. Protein carbonylation is a form of protein oxidation that can be induced by oxidative stress [26, 30]. Increased protein carbonylation was identified in the WAT and gastrocnemius muscle tissues in KO mice, compared to the WT (Figure 3A and

3B). These results are consistent with our previous observation in the liver [26]. Significant increases in heat shock protein 60 (HSP60), a mitochondrial oxidative stress marker, were demonstrated in liver, WAT, and muscle from KO mice, compared to the WT (Figure 3C).

Next, we asked whether BCO2 deficiency was associated with alterations in immune homeostasis. Therefore, we examined the immune cell population changes in the bone marrow of KO mice. Flow cytometry results indicated that KO mice had increases in NK cell numbers (Figure 3D) and the ratio of M1 to M2 macrophages (Figure 3E), but decreases in CD4⁺ and CD8⁺ T cell populations (Figure 3F), compared to the WT. The increase in M1/M2 macrophages may indicate M1 macrophage homing from peripheral tissues and the central circulation. We also identified modulate, but significant elevations of circulating inflammatory markers, including CRP, TNF- α , MCP-1, IL-6, and IL-1 β in KO mice, compared to the WT (Figure 3G).

Collectively, deficiency of BCO2 led to the disruption of mitochondrial respiratory supercomplex assembly, overproduction of mitochondrial superoxide radicals, mitochondrial oxidative stress, protein carbonylation, immune cells activation, and systemic low-grade inflammation in KO mice.

Deficiency of BCO2 elevates blood glucose through the promotion of gluconeogenesis and diminishing of glucose uptake by peripheral tissues

We assessed whether BCO2 deficiency-linked mitochondrial dysfunction and systemic low-grade inflammation are associated with metabolic disorders. First, we characterized glucose metabolism in KO mice. Fasting blood glucose results revealed the elevation of blood glucose levels in mice with BCO2 deficiency (Supplemental Figure S2A). These KO mice developed glucose intolerance compared to those in WT mice, as tested by GTT (Supplemental Figure S2B). Immunoblotting results from liver samples further showed the enhanced expression of mTOR1, FOXO1, PCK1, and PCK2 proteins in liver of KO mice, compared to the WT (Supplemental Figure S2C), indicative of BCO2 deficiency-induced metabolic stress and promotion of gluconeogenesis.

Further, decreases in glucose transporter 4 (GLUT4) protein levels in gastrocnemius muscle and WAT in KO mice (Supplemental Figure S2D), compared to WT, suggest the suppression of glucose uptake by these peripheral tissues (Supplemental Figure S2D). Moreover, we dissected the signaling cascades of GLUT4 trafficking to the plasma membrane in gastrocnemius muscle by immunoblotting. As shown in Supplemental Figure S3, enhanced phosphorylation occurred in insulin receptor substrate 1 (IRS1) on Ser636/639, AKT on Thr308, Ca²⁺/calmodulin kinase II (CaMKII) on Thr286, and Akt substrate of 160 kDa (AS160) on Ser588 in KO mice, compared to the WT. Phosphorylation of AS160 on Ser588 has been confirmed as an essential indicator of Glut4 translocation to the plasma membrane [46]. Elevation of cAMP-dependent protein kinase catalytic subunit (PKA-C) protein levels were also identified in BCO2 KO mice compared to the WT. These results indicated that the trafficking of Glut4 from the Glut4 storage vesicle (GSV) to the plasma membrane was enhanced.

Deficiency of BCO2 is associated with dyslipidemia and impaired lipid metabolism in the liver

We investigated the alteration in lipid metabolism in BCO2 deficient mice. Plasma contents of total CHOL and HDL-C were decreased, but LDL-C and NEFA were elevated in KO mice compared to the WT. However, there was no difference in plasma TG contents between WT and KO mice (Figure 4A).

The liver is the primary organ for lipid synthesis, repackaging of lipoprotein particles, and lipid export. In this study, the KO mice had greater liver weights compared to age- and sex-matched WT mice (Figure 4B), though the liver TG levels were not significantly increased ($P=0.078$, Figure 4C). Several regulators related to lipid metabolism were then assessed in liver samples by immunoblotting. Hepatic levels of sterol regulatory element-binding protein 1c (SREBP1c), acetyl CoA carboxylase (ACC), and apolipoprotein B (ApoB) proteins were elevated in KO mice, compared to the WT (Figure 4D), indicating potentiated lipid synthesis and delivering capacity from the liver to the circulating system and peripheral tissues. Levels of hepatic IRS1 phosphorylation at Ser636/639 were consistent between KO and WT (Figure 4D). The global metabolomics results showed that hepatic contents of diacylglycerol (DAG) (including 1,2-DPG and 1,3-DPG) and HMG were significantly higher, but squalene was significantly lower in KO liver than in the WT (Figure 4E). Moreover, hepatic HMG CoA reductase (HMGCR) protein levels were also suppressed (Figure 4F). According to recent publications, deletion of BCO2 inhibits phosphorylation and activation of AMP-activated protein kinase α (AMPK α) [26, 27, 34], which could further contribute to inhibit the expression of HMGCR [47]. Taken together, deficiency of BCO2 potentiated fatty acid synthesis and DAG production and inhibited CHOL synthesis via suppression of HMGCR (Figure 4G).

Deficiency of BCO2 alters lipid metabolism and stimulates inflammation in WAT

In addition to the liver, adipose tissue is another major endocrine organ involved in lipid metabolism. At the whole-body level, no significant difference in whole-body fat percent was observed between WT and KO mice at 6 weeks of age (Figure 5A). However, histological analysis of the WAT revealed that KO mice had a significant increase in the number of larger ($> 50 \mu\text{m}$ in diameter) adipose cells compared to the WT (Figure 5B). Immunoblotting results further revealed significant decreases in perilipin, peroxisome proliferator-activated receptor γ (PPAR γ), and fatty acid synthase (FASN) in the adipocytes of KO mice, compared to the WT (Figure 5C). In addition, adipose adiponectin mRNA and plasma adiponectin protein levels were declined in BCO2 KO mice compared to the WT (Figure 5D and F), which is suggestive of suppression of lipid droplet mobilization and fatty acid storage and significant hypertrophy in adipocytes. Moreover, BCO2 deficient adipose tissues contained higher numbers of IL6Ra⁺ NK cells and F4/80⁺ cells (Figure 5E and G). Real-time PCR results confirmed the enhanced mRNA expression of inflammatory markers, such as *TNF- α* , *F4/80*, *CD11c*, *MCP-1*, *MIP-1 α* , *VCAM1*, *IL-1 β* , and *IL-10* in WAT of BCO2 KO mice, compared to the WT, as determined by flow cytometry, immunohistochemistry, and real-time PCR, respectively (Figure 5 E–G, Supplemental Figure S4). Together, KO mice had adipocyte hypertrophy, immune cell infiltration, and local inflammation in adipocytes.

Deficiency of BCO2 increases the susceptibility to obesity and diabetes

As shown in Figure 6A and 6B, the HF diet induced the highest levels of fasting blood glucose in KO mice than other groups, e.g., WT fed HF (WT-HF), KO fed LF (KO-LF), and WT fed LF (WT-LF). KO fed HF (KO-HF) had the highest whole-body fat %, compared to other groups.

Commonly, 129S6 mice are recognized as diet-induced obesity (DIO)-resistant mouse strain, while C57BL/6J (B6) is a DIO-sensitive strain [48,49]. Given that deficiency of BCO2 in 129S6 mice (e.g., KO, homozygous) did not increase the whole-body fat % (Figure 5B, WT-LF vs KO-LF), we determined the effect of BCO2 deficiency on the change of whole-body fat % in B6 background mice fed an LF diet (named as KO(B6), homozygous). The results indicated that male KO(B6) mice had a significant increase in whole-body fat %, compared to their genetic background strain, e.g., WT(B6) (Figure 6C).

Further, KO(B6) homozygous mice were crossed with *LepR* knockout (db/db) heterozygous (Het). Various offsprings were genotyped and fasting blood glucose levels were monitored at 4 weeks of age. The results revealed that male mice with double knockout of *BCO2* and *LepR* homozygous strain (KO(B6)/db/db) had the highest fasting blood glucose level compared to other groups, e.g., WT(B6), KO(B6), db/db, and/or double knockout Het mice (Figure 6D). Data suggested that deficiency of BCO2 made mice more susceptible to DIO and diabetes.

Mito-TEMPO attenuates BCO2 deficiency-induced low-grade inflammation

Mito-TEMPO is a specific scavenger of mitochondrial ROS, including superoxide radicals [50]. To determine whether BCO2 deficiency-induced mitochondrial oxidative stress and inflammation can be rescued, Mito-TEMPO was applied to the primary MEFs in culture and mice in vivo.

The results of 8-OHdG immunofluorescence indicated that 8-OHdG signals were stronger in BCO2 KO MEFs, compared to the WT MEFs, which could be diminished by Mito-TEMPO at 2 $\mu\text{mol/L}$ (Supplemental Figure S5A). A higher dose of Mito-TEMPO at 20 $\mu\text{mol/L}$ induced stronger 8-OHdG signals in both types of MEFs, suggesting the toxicity of 8-OHdG at 20 $\mu\text{mol/L}$. Therefore, we assessed MitoSOX signals in MEFs treated with 2 $\mu\text{mol/L}$ Mito-TEMPO for 1 h. The results showed that Mito-TEMPO quenched MitoSOX signals by up to 55.8 % in primary BCO2 KO MEFs (KO-Tempo vs KO-PBS control, Supplemental Figure S5 B and C).

Next, 6-week old male BCO2 KO were i.p. injected with Mito-TEMPO at 3.5 mg/kg BW/day for 7 consecutive days, injection with PBS as vehicle control. Neither abnormal behaviors nor health problems, such as shading, food intake, and water consumption, was observed in KO mice caused by the administration of Mito-TEMPO, indicating that Mito-TEMPO (for 7 days) was not toxic to mice. As shown in Figure 7, Mito-TEMPO injection significantly decreased plasma inflammatory cytokines, such as TNF- α , IL-6, and IL-1 β (Figure 7A) in KO-Tempo mice, compared to the KO-PBS control. Compared to PBS controls, Mito-TEMPO decreased the population of NK cells and the ratio of M1/M2 macrophages and increased both CD4⁺ and CD8⁺ T cells in the bone marrow of KO-Tempo

mice (Figure 7B). In terms of glucose metabolism, Mito-TEMPO did not significantly lower the fasting blood glucose level or glucose intolerance in KO-Tempo mice, compared to the PBS groups (Figure 7C and D). Although the hepatic mTOR1 protein levels and AMPK α activation were reversed, hepatic expression of PCK1 and PCK2 proteins was not altered by Mito-TEMPO (Figure 7E and Supplemental Figure S5D). No difference was identified in whole-body fat %, WAT NK cell populations, or plasma CHOL, HDL-C, LDL-C, TG, or NEFA contents in KO-Tempo mice, compared to KO-PBS mice (Figure 7F–H).

Collectively, BCO2 deficiency-induced mitochondrial oxidative stress and inflammation could be rescued by the application of mitochondrial specific antioxidants, such as Mito-TEMPO.

Discussion

Recently, enzymatic roles and regulation of BCO2 in carotenoid metabolism in birds and non-primate laboratory animals have been extensively reported in the literature [13–19]. Yet, the functional regulation of BCO2 as a carotenoid metabolic enzyme in human subjects is not well understood [20–22]. Gong *et al.* reported that BCO2 status determines the activation of nuclear factor kappa-light-chain-enhancer of activated B cells signaling pathway in cell cultures [22]. Here, we demonstrated that BCO2, along with mitochondrial respiratory complex proteins and SOD2 were decreased, in liver of type 2 diabetic individuals. Using loss-of-function and rescue approaches, we further demonstrated that BCO2 was critical for mitochondrial respiratory supercomplex assembly. The deficiency of BCO2 caused mitochondrial oxidative stress, which in turn, resulted in low-grade inflammation and impaired metabolic homeostasis.

The importance of BCO2 in the development of metabolic disorders, such as obesity, type 2 diabetes and its complications, is significant but underinvestigated. In the current study, we reported the suppression of *BCO2* mRNA and proteins in the diabetic liver of human subjects. We also demonstrated this suppression is associated with impaired mitochondrial respiration and mitochondrial oxidative stress as determined by decreases in NDUFB6, NDUFB9, and SOD2. In the current mouse models, deficiency of BCO2 caused mice to be more susceptible to DIO and induced the early onset of hyperglycemia in the double knockout mice of *LepR* and *BCO2*, when mice were fed diets with non-detectable carotenoids. It could be possibly predicted that a decrease in BCO2 expression is critical for the alteration of mitochondrial respiration, oxidative stress, and lipid accumulation, the phenotypes commonly identified in type 2 diabetes.

BCO2 can be essential for SC formation. Recent cryo-electron microscopy studies have revealed the structures of SCs, such as I₂+III₂+IV₂. It may or may not associated with complex II [51]. NADH: ubiquinone oxidoreductase subunit A11 (NDUFA11) is a docking protein essential for recruiting CIII and CIV to form SCs [51]. Cytochrome C oxidase subunit 7A2 Like (COX7a2L) and cytochrome C oxidase assembly homolog 15 (COX15) are proteins that have recently been identified as essential components in the formation of III₂+IV and stabilize the supercomplexes [52, 53]. Association of BCO2 deficiency with III₂+IV disassembly may suggest that BCO2 is a new protein critical for III₂+IV assembly

and SC stability, though the precise mechanism by which BCO2 is involved in SC assembly has not been well elucidated.

Mitochondria are highly dynamic organelles in response to stimuli, such as fasting or food depletion. Fasted mice typically form mitochondrial respiratory supercomplexes to yield a higher respiration efficiency, ATP generation, and an optimal ROS production rate [54–58]. SC III₂+IV assembly was largely disrupted by the deficiency of BCO2. That, in turn, could cause the escape of electrons from the electron transport chain and sequential overproduction of superoxide radicals in mitochondria [35, 36]. The latter was confirmed by measures of MitoSOX signals in primary MEFs. Increases in protein carbonylation, mitochondrial HSP60 protein levels, and 8-OHdG signals were indirectly supportive evidence of oxidative stress. Because other SCs with much higher molecular weights were not well separated due to the limited size of BN-PAGE minigels used, there may be other impairments in SC assembly that were not detected. We would expect that BCO2 deficiency-impaired mitochondrial respiration and oxidative stress homeostasis could impact many types of cells that have mitochondria, such as immune cells and hepatocytes.

Mitochondrial oxidative stress contributes to systemic low-grade inflammation by unspecific activation of the host immune response, which is the main source of inflammatory mediators [59]. KO mice had a greater population of NK cells and a higher ratio of M1/M2 macrophages in the bone marrow, though a portion of them could be homing immune cells. On the other hand, animals can compensate for the lower level of CD8⁺ T cells by increasing the proliferation of NK cells [60, 61]. The increased population of NK cells might further contribute to promoting the transition of M2 macrophages to M1 macrophages, which eventually elevated the production of inflammatory cytokines [62].

Mitochondrial oxidative stress reflects an imbalance between the excessive production of ROS and the ability to detoxify the ROS and/or to repair oxidative damage [60]. Mito-TEMPO is a mitochondria-targeted antioxidant, consisting of the lipophilic cation triphenylphosphonium (TPP) with the piperidine nitroxide [50, 63]. TPP functions to penetrate lipid bilayers easily and deposit TEMPO in mitochondria selectively [50, 64]. It has been confirmed both *in vivo* and *in vitro* that Mito-TEMPO presents alkyl radical and superoxide scavenging properties [50, 63, 65]. Interestingly, Mito-TEMPO administration decreased the numbers of NK cells and the ratio of M1/M2 macrophages and increased both CD4⁺ and CD8⁺ T cells in the bone marrow of KO mice. Additionally, Mito-TEMPO lowered the levels of systemic inflammatory cytokines in KO mice. These results supported the concept that BCO2 deficiency-induced mitochondrial oxidative stress is a causal factor for immune dysregulation and systemic low-grade inflammation in KO mice.

Systemic low-grade inflammation is linked to metabolic dysfunction in KO mice. In this current study, KO mice had an elevated blood glucose level and impaired glucose and lipid metabolism. Several possibilities may be responsible for the elevation of fasting blood glucose levels in KO mice. For example, loss of BCO2 remodels the hypothalamic mitochondrial function leading to an increase in the food intake [26]. Deficiency of BCO2 triggered mitochondrial oxidative stress, which might impair the insulin signaling pathway and inhibit the uptake of glucose by peripheral tissues, such as skeletal muscle and WAT.

Moreover, mitochondrial oxidative stress might stimulate gluconeogenesis in the liver of KO mice.

In contrast, there could be a compensatory mechanism in terms of low Glut4 expression in KO mice by stimulating the translocation of Glut4 from GSVs in the cytosol to the plasma membrane [46], which can be accomplished by oxidative stress-enhanced phosphorylation of AS160 (Supplemental Figure S2). However, the 7-day Mito-TEMPO administration could not completely rescue KO mice from the elevation of fasting blood glucose and lipid markers and insulin resistance. It may indicate that mitochondrial oxidative stress is not a sole causal factor in the elevation of blood glucose. However, the reversal of mTOR1 and AMPK α activation may also suggest that the current Mito-TEMPO treatment is not adequate to recover the whole-body metabolism in KO mice. A longer period of the Mito-TEMPO treatments, such as 4 weeks has been reported in mouse models [50].

The deficiency of BCO2 caused adipocyte inflammation and hypertrophy. It has recently been reported that obese human subjects have a particular subpopulation of NK cells in abdominal fat, defined as IL6Ra/CD126⁺ NK cells [41]. In KO adipocytes, a higher population of IL6Ra/CD126⁺ NK cells indicated local inflammation and NK cell infiltration into adipose tissues, compared to the WT. Perilipin is a major phosphoprotein found on the surface of lipid droplets in adipocytes. It acts as a gatekeeper to prevent the release of NEFA from hydrolyzing TG by lipases [66, 67]. Suppression of perilipins promotes the release of NEFA into the circulation by increasing the basal rate of lipolysis [68, 69] and eventually leads to fewer but larger lipid droplets in the adipocyte [70]. In the current study, suppression of perilipin could account for adipocyte hypertrophy and elevation of circulatory NEFA in KO mice. Adipocyte hypertrophy could also promote the infiltration of immune cells, such as NK cells in KO mice.

In summary, our results demonstrate that BCO2 is essential for mitochondrial respiration, which is critical for immunity and whole-body metabolic homeostasis in mammals. This study further may provide insights into potential therapeutic roles of BCO2 in the prevention of chronic, low-grade inflammation and associated metabolic disorders, such as obesity and diabetes. Although there were no detectable carotenoids in the diets and animals, we could not exclude the possibility of trace levels of carotenoids and apo-carotenoids existing which may act as confounding factors in the current study.

Supplementary Material

Refer to Web version on PubMed Central for supplementary material.

Acknowledgments and Funding Information

The authors thank Dr. Johannes von Lintig at Case Western Reserve University for the generous gift of the original BCO2 knockout mouse. We thank Sandra Peterson for the technical support and laboratory management. Flow cytometry was conducted in the Immunopathology Core in the OCRID at Oklahoma State University.

Funding: This work was partially supported by the National Institute of Food and Agriculture, USDA [grant number 2020-67017-30842]. Research reported in this publication was partially supported by the National Institute of General Medical Sciences of the National Institutes of Health under Award Number P20GM103648. The content

is solely the responsibility of the authors and does not necessarily represent the official views of the National Institutes of Health.

Abbreviations

| | |
|--------------------------------|--|
| 1,2-DPG | 1,2-dipalmitoylglycerol |
| 1,3-DPG | 1,3-dipalmitoylglycerol |
| 8-OHdG | 8-hydroxy-2-deoxyguanosine |
| ACC | acetyl-CoA carboxylase |
| I | respiratory complex I, or CI |
| II | respiratory complex II, or CII |
| III | respiratory complex III, or CIII |
| III₂ | respiratory complex III dimer, or CIII ₂ |
| III₂ +IV | supercomplex III ₂ and IV |
| IV | respiratory complex IV, or CIV |
| AKT2 | AKT Serine/Threonine Kinase 2 |
| AMPKα | AMP-activated protein kinase α |
| ApoB | apolipoprotein B |
| AS160 | AKT substrate of 160kDa |
| B6 | C57BL/6J |
| BCO2 | β -carotene oxygenase 2 |
| BN-PAGE | blue-native PAGE |
| BW | body weight |
| CI-CV | mitochondrial respiratory complex I to complex V |
| CaMKII | Ca ²⁺ /calmodulin-dependent protein kinase II |
| CD11c | integrin alpha X |
| CRP | C-reactive protein |
| DAPI | 4',6-diamidino-2-phenylindole |
| DAG | diacylglycerol |
| DIO | diet-induced obesity |
| db/db | leptin receptor knockout mice |

| | |
|-------------------------------|---|
| DNPH | 2,4-dinitrophenylhydrazone |
| F4/80 | EGF-like module-containing mucin-like hormone receptor-like 1 |
| FASN | fatty acid synthase |
| FBG | fasting blood glucose |
| FOXO1 | forkhead box protein O1 |
| GAPDH | glyceraldehyde-3-phosphate dehydrogenase |
| Glut4 | glucose transporter 4 |
| GSV | glut4 storage vesicle |
| GTT | glucose tolerance test |
| hBCO2 | human BCO2 variant 1 |
| HDL-C | high-density lipoprotein cholesterol |
| HF | high-fat diet |
| Het | heterozygous |
| HMG | 3-hydroxy-3-methylglutarate |
| HMGCR | HMG-CoA reductase |
| HMGCS | HMG-CoA synthase |
| HSP60 | 60 kDa heat shock protein |
| IL-1β | interleukin 1 β |
| IL-6 | interleukin 6 |
| IL-10 | interleukin 10 |
| IL-18 | interleukin 18 |
| IL6Ra | IL-6 receptor subunit α |
| IRS1 | insulin receptor substrate 1 |
| ITT | insulin tolerance test |
| KO | knockout |
| LDL-C | low-density lipoprotein cholesterol |
| LepR | leptin receptor |
| LF | low-fat diet |

| | |
|---------------------------------|--|
| mBCO2 | mouse BCO2 |
| MCP-1 | monocyte chemoattractant protein-1 |
| Mito-TEMPO | (2-(2,2,6,6-Tetramethylpiperidin-1-oxyl-4-ylamino)-2-oxoethyl) triphenyl-phosphonium chloride, monohydrate |
| MEF | mouse embryonic fibroblast |
| MIP-1α | macrophage inflammatory protein 1 α |
| MTCO2 | mitochondrial encoded cytochrome C oxidase II |
| mTOR1 | mammalian target of rapamycin 1 |
| NDUFB6 | NADH:ubiquinone oxidoreductase subunit B6 |
| NDUFB9 | NADH:ubiquinone oxidoreductase subunit B9 |
| NEFA | non-esterified fatty acids |
| NK cells | natural killer cells |
| PBS | phosphate-buffered saline |
| PCK1/2 | phosphoenolpyruvate carboxykinase 1/2 |
| PKA-C | cAMP-dependent protein kinase catalytic subunit |
| PPARγ | peroxisome proliferator-activated receptor γ |
| ROS | reactive oxygen species |
| SC | supercomplex |
| SM | skeletal muscle |
| SOD2 | superoxide dismutase [Mn], mitochondrial |
| SREBP1c | sterol regulatory element-binding protein 1 c |
| TG | triglyceride |
| TNF-α | tumor necrosis factor α |
| UQCRC2 | ubiquinol-cytochrome reductase core protein II |
| VCAM1 | vascular cell adhesion protein 1 |
| WAT | white adipose tissue |
| WT | wild type |

References

1. Antonelli M, Kushner I. It's time to redefine inflammation. *FASEB J* 2017; 31: 1787–1791 (2017). doi: 10.1096/fj.201601326R [PubMed: 28179421]
2. Ellulu MS, Patimah I, Khaza'ai H, et al.. Obesity and inflammation: the linking mechanism and the complications. *Arch Med Sci* 2017; 13(4): 851–863. doi: 10.5114/aoms.2016.58928 [PubMed: 28721154]
3. Zatterale F, Longo M, Naderi J, et al.. Chronic adipose tissue inflammation linking obesity to insulin resistance and type 2 diabetes. *Front Physiol* 2020; 10.3389/fphys.2019.01607
4. Furman D, Campisi J, Verdin E et al. Chronic inflammation in the etiology of disease across the life span. *Nat Med* 25, 1822–1832 (2019). 10.1038/s41591-019-0675-0 [PubMed: 31806905]
5. Margin D, Ungurianu A, Purdel C, et al. Chronic inflammation in the context of everyday life: Dietary changes as mitigating factors.. *Int J Environ Res Public Health* 2020;17(11):4135. doi: 10.3390/ijerph17114135.
6. Minihane AM, Vinoy S, Russell WR., et al.. Low-grade inflammation, diet composition and health: current research evidence and its translation. *Br J Nutr.* 2015 10 14; 114(7): 999–1012. doi: 10.1017/S0007114515002093 [PubMed: 26228057]
7. Temkin AM, Bowers RR, Ulmer CZ et al. Increased adiposity, inflammation, metabolic disruption and dyslipidemia in adult male offspring of DOSS treated C57BL/6 dams. *Sci Rep* 9, 1530 (2019). 10.1038/s41598-018-38383-9 [PubMed: 30728429]
8. Weinberg SE, Sena LA, Chandel NS. Mitochondria in the regulation of innate and adaptive immunity. *Immunity.* 2015;42(3):406–417. doi:10.1016/j.immuni.2015.02.002 [PubMed: 25786173]
9. Angajala A, Lim S, Joshua B. Phillips JB, et al.. Diverse roles of mitochondria in immune responses: Novel insights into immuno-metabolism, *Front Immunol* 2018 10.3389/fimmu.2018.01605
10. Indo HP, Yen HC, Nakanishi I, et al. A mitochondrial superoxide theory for oxidative stress diseases and aging. *J Clin Biochem Nutr.* 2015;56(1):1–7. doi:10.3164/jcbs.14-42 [PubMed: 25834301]
11. Brand MD. The sites and topology of mitochondrial superoxide production. *Exp Gerontol.* 2010;45(7–8):466–472. doi:10.1016/j.exger.2010.01.003 [PubMed: 20064600]
12. Moshfegh CM, Collins CW, Gunda V, et al.. Mitochondrial superoxide disrupts the metabolic and epigenetic landscape of CD4+ and CD8+ T-lymphocytes. *Redox Biol* 2019; 27: 101141. 10.1016/j.redox.2019.101141 [PubMed: 30819616]
13. Amengual J, Lobo GP, Golczak M, et al.. A mitochondrial enzyme degrades carotenoids and protects against oxidative stress. *FASEB J* 2011; 25:948–959. [https://doi:10.1016/j.expneurol.2017.02.001](https://doi.org/10.1016/j.expneurol.2017.02.001). [PubMed: 21106934]
14. Wyss A Carotene oxygenases: a new family of double bond cleavage enzymes. *J Nutr* 2004;134(1):246S–250S. doi: 10.1093/jn/134.1.246S. [PubMed: 14704328]
15. von Lintig J, Hessel S, Isken A, et al.. Towards a better understanding of carotenoid metabolism in animals. *Biochim Biophys Acta* 2005;1740(2):122–31. doi: 10.1016/j.bbadis.2004.11.010. [PubMed: 15949678]
16. Hu KQ, Liu C, Ernst H, Krinsky NI, Russell RM, Wang XD. The biochemical characterization of ferret carotene-9',10'-monooxygenase catalyzing cleavage of carotenoids in vitro and in vivo. *J Biol Chem* 2006;281(28):19327–38. doi: 10.1074/jbc.M512095200. [PubMed: 16672231]
17. Fallahshahroudi A, Sorato E, Altimiras J, Jensen P. The domestic BCO2 allele buffers low-carotenoid diets in chickens: Possible fitness increase through species hybridization. *Genetics* 2019;212(4):1445–1452. doi: 10.1534/genetics.119.302258. [PubMed: 31160321]
18. Gazda MA, Toomey MB, Araújo PM, et al. Genetic basis of de novo appearance of carotenoid ornamentation in bare parts of canaries. *Molr Biol Evolu* 2020; 37(5): 1317–1328. 10.1093/molbev/msaa006
19. Gazda MA, Araújo PM, Lopes RJ, et al.. A genetic mechanism for sexual dichromatism in birds. *Science* 2020;368(6496):1270–1274. doi: 10.1126/science.aba0803. [PubMed: 32527835]

20. Li B, Vachali PP, Gorusupudi A, et al.. Inactivity of human β,β -carotene-9',10'-dioxygenase (BCO2) underlies retinal accumulation of the human macular carotenoid pigment.. Proc Natl Acad Sci U S A 2014;111(28):10173–8. doi: 10.1073/pnas.1402526111. [PubMed: 24982131]
21. Babino D, Palczewski G, Widjaja-Adhi MA, Kiser PD, Golczak M, von Lintig J. Characterization of the Role of β -Carotene 9,10-Dioxygenase in Macular Pigment Metabolism. J Biol Chem 2015;290(41):24844–57. doi: 10.1074/jbc.M115.668822. [PubMed: 26307071]
22. Gong X, Marisiddaiah R, Zaripheh S, et al. Mitochondrial beta-carotene 9, 10 oxygenase modulates prostate cancer growth via NF-kappa B inhibition: a lycopene-independent function. Mol Cancer Res 2016;14:966–975. https://doi:10.1158/1541-7786.MCR-16-0075. [PubMed: 27406826]
23. He M, Cornelis MC, Kraft P, et al.. Genome-wide association study identifies variants at the IL18-BCO2 locus associated with interleukin-18 levels. Arterioscler Thromb Vasc Biol 2010;30:885–890. https://doi:10.1161/ATVBAHA.109.199422. [PubMed: 20150558]
24. Meyers KJ, Mares JA, Igo RP, et al.. Genetic evidence for role of carotenoids in age-related macular degeneration in the Carotenoids in Age-Related Eye Disease Study (CAREDS). Invest Ophthalmol Vis Sci 2014;55:587–599. https://doi:10.1167/iovs.13-13216. [PubMed: 24346170]
25. Brocato J, Hernandez M, Laulicht F, et al. In vivo exposures to particulate matter collected from Saudi Arabia or nickel chloride display similar dysregulation of metabolic syndrome genes. J Toxicol Environ Health A 2015;78:1421–1436. https://doi:10.1080/15287394.2015.1095689. [PubMed: 26692068]
26. Wu L, Guo X, Hartson SD, et al., Lack of $\beta\beta$ -carotene-9', 10'-oxygenase 2 leads to hepatic mitochondrial dysfunction and cellular oxidative stress in mice. Mol Nutr Food Res 2016 12 19. https://doi:10.1002/mnfr.201600576.
27. Guo X, Wu L, Lyu Y, et al.. Ablation of β,β -carotene-9',10'-oxygenase 2 remodels the hypothalamic metabolome leading to metabolic disorders in mice. J Nutr Biochem 2017;46:74–82. https://doi:10.1016/j.jnutbio.2017.02.019. [PubMed: 28482236]
28. Kieffer TJ, Heller RS, Habener JF. Leptin receptors expressed on pancreatic beta-cells. Biochem Biophys Res Commun 1996;224(2):522–7. doi: 10.1006/bbrc.1996.1059. [PubMed: 8702421]
29. Durkin ME, Qia X, Popescu NC, Lowy DR. Isolation of mouse embryo fibroblasts. Bio-protocol 2013; 3(18): e908. DOI: 10.21769/BioProtoc.908 [PubMed: 27376106]
30. Strong MD, Hart MD, Tang TZ, et al.. Role of zinc transporter ZIP12 in susceptibility-weighted brain magnetic resonance imaging (MRI) phenotypes and mitochondrial function. FASEB J 2020 7 27. doi: 10.1096/fj.202000772R.
31. Yao HR, Liu J, Plumeri D, et al. Lipotoxicity in HepG2 cells triggered by free fatty acids. Am J Transl Res. 2011;3(3):284–291. [PubMed: 21654881]
32. Yang S, Park H, Kim J et al. Mito-TEMPO improves development competence by reducing superoxide in preimplantation porcine embryos. Sci Rep 8, 10130 (2018). 10.1038/s41598-018-28497-5 [PubMed: 29973637]
33. Galarraga M, Campión J, Muñoz-Barrutia A, et al. Adiposoft: automated software for the analysis of white adipose tissue cellularity in histological sections [published correction appears in J Lipid Res. 2014 Dec;55(12):2705]. J Lipid Res. 2012;53(12):2791–2796. doi:10.1194/jlr.D023788 [PubMed: 22993232]
34. Wu L, Guo X, Lyu Y, et al.. Targeted metabolomics reveals abnormal hepatic energy metabolism by depletion of β -carotene oxygenase 2 in mice. Sci Rep 2017;7(1):14624. doi: 10.1038/s41598-017-15222-x. [PubMed: 29116185]
35. Lopez-Fabuel I, Le Douce J, Logan A, et al.. Complex I assembly into supercomplexes determines differential mitochondrial ROS production in neurons and astrocytes. Proc Natl Acad Sci U S A 2016;113:13063–13068. https://doi:10.1073/pnas.1613701113. [PubMed: 27799543]
36. Lapuente-Brun E, Moreno-Loshuertos R, Acín-Pérez R, et al.. Supercomplex assembly determines electron flux in the mitochondrial electron transport chain. Science 2013;340(6140):1567–70. doi: 10.1126/science.1230381. [PubMed: 23812712]
37. Trouplin V, Boucherit N, Gorvel L, Conti F, Mottola G, Ghigo E. Bone marrow-derived macrophage production. J Vis Exp 2013;81: e50966. doi: 10.3791/50966

38. Zhang X, Goncalves R, Mosser DM. The isolation and characterization of murine macrophages. *Curr Protoc Immunol* Chapter 14, Unit 14 11 (2008).
39. Poli A, Michel T, Theresine M, Andres E, Hentges F, Zimmer J. CD56bright natural killer (NK) cells: an important NK cell subset. *Immunol* 2009;126:458–465. doi: 10.1111/j.1365-2567.2008.03027.x.
40. Jablonski KA, Amici SA, Webb LM, et al.. Novel markers to delineate murine M1 and M2 macrophages. *PLoS One* 2015;10, e0145342. doi: 10.1371/journal.pone.0145342. [PubMed: 26699615]
41. Theurich S, Tsaousidou E, Hanssen R, et al.. IL-6/Stat3-dependent induction of a distinct, obesity-associated NK cell subpopulation deteriorates energy and glucose homeostasis. *Cell Metab* 2017; 26, 171–184 e176. doi: 10.1016/j.cmet.2017.05.018. [PubMed: 28683285]
42. Thaïss CA, Levy M, Grosheva I, et al.. Hyperglycemia drives intestinal barrier dysfunction and risk for enteric infection. *Science* 2018; 359(6382):1376–1383. doi: 10.1126/science.aar3318. [PubMed: 29519916]
43. Shibata S, Shibata N, Shibata T, Sasaki H, Singh DP, Kubo E. The role of Prdx6 in the protection of cells of the crystalline lens from oxidative stress induced by UV exposure. *Jpn J Ophthalmol* 2016; 60, 408–418. doi: 10.1007/s10384-016-0461-1. [PubMed: 27379999]
44. Schmittgen TD, Livak KJ. Analyzing real-time PCR data by the comparative C(T) method. *Nat Protoc* 2008; 3:1101–1108. doi: 10.1038/nprot.2008.73. [PubMed: 18546601]
45. Suthammarak W, Somerlot BH, Opheim E, Sedensky M, Morgan PG. Novel interactions between mitochondrial superoxide dismutases and the electron transport chain. *Aging Cell* 2013;12(6):1132–40. doi: 10.1111/acer.12144. [PubMed: 23895727]
46. Bai L, Wang Y, Fan J, Chen Y, Ji W, Qu A, Xu P, James DE, Xu T. Dissecting multiple steps of GLUT4 trafficking and identifying the sites of insulin action. *Cell Meta* 2007;5(1):47–57. doi: 10.1016/j.cmet.2006.11.013.
47. Liu S, Jing F, Yu C, Gao L, Qin Y, Zhao J. AICAR-induced activation of AMPK inhibits TSH/SREBP-2/HMGCR pathway in liver. *PloS One* 2015;10, e0124951. doi: 10.1371/journal.pone.0124951. [PubMed: 25933205]
48. Fink BD, Herlein JA, Almind K, et al.. Mitochondrial proton leak in obesity-resistant and obesity-prone mice. *AM J Physiol Regul Integr Comp Physiol* 2007;293(5):R1773–80. doi: 10.1152/ajpregu.00478.2007. [PubMed: 17761507]
49. Almind K, Kahn CR. Genetic determinants of energy expenditure and insulin resistance in diet-induced obesity in mice. *Diabetes* 2004;53(12):3274–85. doi: 10.2337/diabetes.53.12.3274. [PubMed: 15561960]
50. Ni R, Cao T, Xiong S, et al.. Therapeutic inhibition of mitochondrial reactive oxygen species with mito-TEMPO reduces diabetic cardiomyopathy. *Free Radic Biol Med* 2016;90, 12–23. doi: 10.1016/j.freeradbiomed.2015.11.013. [PubMed: 26577173]
51. Guo R, Zong S, Wu M, Gu J, Yang M.. Architecture of human mitochondrial respiratory megacomplex I₂ III₂ IV₂. *Cell* 2017;170(6):1247–1257.e12. doi: 10.1016/j.cell.2017.07.050. [PubMed: 28844695]
52. Pérez-Pérez R, Lobo-Jarne T, Milenkovic D, Mourier A, Bratic A, García-Bartolomé A, Fernández-Vizarrá E, Cadenas S, Delmiro A, García-Consuegra I, Arenas J, Martín MA, Larsson NG, Ugalde C.. COX7A2L is a mitochondrial complex III binding protein that stabilizes the III₂+IV supercomplex without affecting respirasome formation. *Cell Rep* 2016;16(9):2387–98. doi: 10.1016/j.celrep.2016.07.081. [PubMed: 27545886]
53. Herwaldt EJ, Rivett ED, White AJ, Hegg EL.. Cox15 interacts with the cytochrome bc (1) dimer within respiratory supercomplexes as well as in the absence of cytochrome c oxidase. *J Biol Chem* 2018;293(42):16426–16439. doi: 10.1074/jbc.RA118.002496. [PubMed: 30181213]
54. Calvo E, Cogliati S, Hernansanz-Agustín P, et al.. Functional role of respiratory supercomplexes in mice: SCAF1 relevance and segmentation of the Q(pool). *Sci Adv* 2020;6(26):eaba7509. doi: 10.1126/sciadv.aba7509. [PubMed: 32637615]
55. Acin-Perez R, Enriquez JA. The function of the respiratory supercomplexes: the plasticity model. *Biochim Biophys Acta* 2014;1837(4):444–50. doi: 10.1016/j.bbabi.2013.12.009. [PubMed: 24368156]

56. Jang S, Javadov S. Association between ROS production, swelling and the respirasome integrity in cardiac mitochondria. *Arch Biochem Biophys* 2017;630:1–8. doi: 10.1016/j.abb.2017.07.009. [PubMed: 28736227]
57. Diaz F, Enríquez JA, Moraes CT. Cells lacking Rieske iron-sulfur protein have a reactive oxygen species-associated decrease in respiratory complexes I and IV. *Mol Cell Biol* 2012;32(2):415–29. doi: 10.1128/MCB.06051-11. [PubMed: 22106410]
58. Garaude J, Acín-Pérez R, Martínez-Cano S, et al.. Mitochondrial respiratory-chain adaptations in macrophages contribute to antibacterial host defense. *Nat Immunol* 2016;17(9):1037–1045. doi: 10.1038/ni.3509. [PubMed: 27348412]
59. Jin L, Lenz LL, Cambier JC. Cellular reactive oxygen species inhibit MPYS induction of IFN β . *PLoS One* 2010, e15142. doi: 10.1371/journal.pone.0015142. [PubMed: 21170271]
60. Johnson TR, Hong E, Van Kaer L, Koezuka Y, Graham BS. NK T cells contribute to expansion of CD8(+) T cells and amplification of antiviral immune responses to respiratory syncytial virus. *J Virol* 2002;76(9):4294–303. doi: 10.1128/jvi.76.9.4294-4303.2002. [PubMed: 11932395]
61. Anderson CK, Reilly EC, Lee AY, Brossay L. Qa-1-restricted CD8 + T Cells can compensate for the absence of conventional T cells during viral infection. *Cell Rep* 2019;27(2):537–548.e5. doi: 10.1016/j.celrep.2019.03.059. [PubMed: 30970256]
62. Bellora F, Castriconi F, Dondero A, et al.. The interaction of human natural killer cells with either unpolarized or polarized macrophages results in different functional outcomes. *PNAS* 2010; 107(50): 21659–21664; 10.1073/pnas.1007654108 [PubMed: 21118979]
63. Liang HL, Sedlic F, Bosnjak Z, Nilakantan V. SOD1 and MitoTEMPO partially prevent mitochondrial permeability transition pore opening, necrosis, and mitochondrial apoptosis after ATP depletion recovery. *Free Radic Biol Med* 2010;49(10):1550–60. doi: 10.1016/j.freeradbiomed.2010.08.018. [PubMed: 20736062]
64. Trnka J, Blaikie FH, Smith RA, Murphy MP. A mitochondria-targeted nitroxide is reduced to its hydroxylamine by ubiquinol in mitochondria. *Free Radic Biol Med* 2008; 44:1406–1419. doi: 10.1016/j.freeradbiomed.2007.12.036. [PubMed: 18206669]
65. Liu M, Liu H, Dudley SC. Reactive oxygen species originating from mitochondria regulate the cardiac sodium channel. *Circ Res* 2010;107(8):967–74. doi: 10.1161/CIRCRESAHA.110.220673. [PubMed: 20724705]
66. Thiam AR, Farese RV Jr, Walther TC. The biophysics and cell biology of lipid droplets. *Nat Rev Mol Cell Biol* 2013;14(12):775–86. doi: 10.1038/nrm3699. [PubMed: 24220094]
67. Jacquier N, Mishra S, Choudhary V, Schneider R. Expression of oleosin and perilipins in yeast promotes formation of lipid droplets from the endoplasmic reticulum. *J Cell Sci* 2013;126(Pt 22):5198–209. doi: 10.1242/jcs.131896. [PubMed: 24006263]
68. Zhang HH, Souza SC, Muliro KV, Kraemer FB, Obin MS, Greenberg AS. Lipase-selective functional domains of perilipin A differentially regulate constitutive and protein kinase A-stimulated lipolysis. *J Biol Chem* 2003;278(51):51535–42. doi: 10.1074/jbc.M309591200 [PubMed: 14527948]
69. Wang Y, Sullivan S, Trujillo M, et al.. Perilipin expression in human adipose tissues: Effects of severe obesity, gender, and depot. *Obes Res* 2003;11(8):930–6. doi: 10.1038/oby.2003.128. [PubMed: 12917496]
70. Bell M, Wang H, Chen H, et al.. Consequences of lipid droplet coat protein downregulation in liver cells abnormal lipid droplet metabolism and induction of insulin resistance. *Diabetes* 2008;57(8):2037–45. doi: 10.2337/db07-1383. [PubMed: 18487449]

Highlight

1. *BCO2* mRNA and protein levels are decreased in liver of type 2 diabetic human subjects
2. *BCO2* deficient mice are more susceptible to diet-induced obesity and type 2 diabetes
3. Deficiency of *BCO2* impairs mitochondrial respiratory supercomplex assembly
4. Deficiency of *BCO2* stimulates superoxide overproduction in mitochondria
5. Mito-TEMPO attenuates *BCO2* deficiency-induced low-grade inflammation in mice

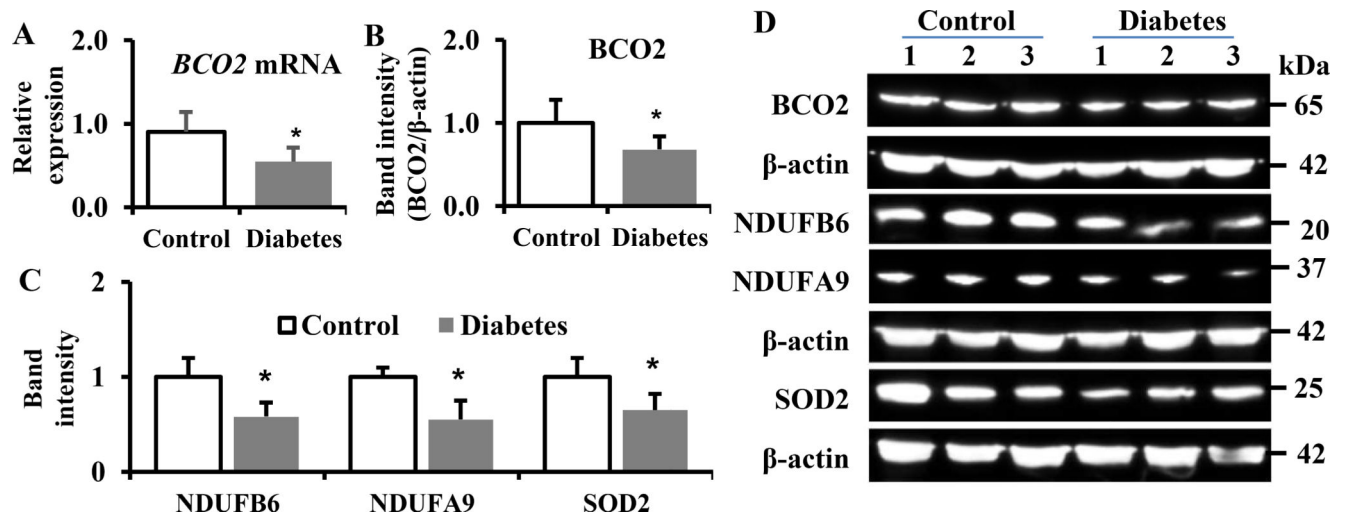


Figure 1. Expression of BCO2 is decreased in human diabetic liver specimens

Total RNA and protein lysates were extracted from three type 2 diabetic human liver specimens and healthy controls and subject to real-time PCR and immunoblotting. **A**, *BCO2* mRNA expression. **B**, Relative *BCO2* protein levels. **C**, Protein expression levels of NDUFB6, NDUFA9, and SOD2. **D**, Representative images of immunoblotting. Values are means \pm S.D., n=3 with 2 technical replicates. * Different from control (e.g., healthy liver samples), $P < 0.05$. *BCO2*, β -carotene oxygenase 2; NDUFA9, NADH:ubiquinone oxidoreductase subunit A9; NDUFB6, NADH:ubiquinone oxidoreductase subunit B6; SOD2, superoxide dismutase 2, mitochondrial

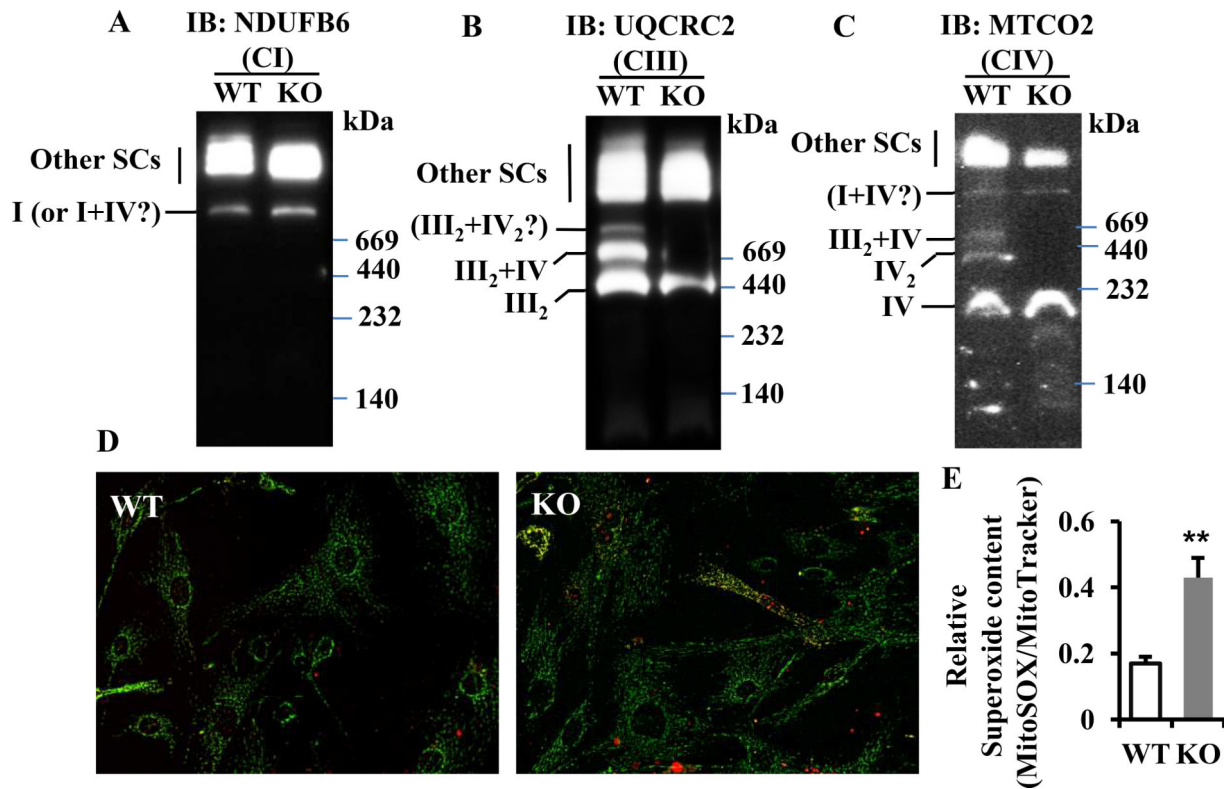


Figure 2. Deficiency of BCO2 disrupts mitochondrial respiratory supercomplex assembly and stimulates mitochondrial superoxide production

Mitochondrial enriched fractions were isolated from the liver of 6-week old male β -carotene oxygenase 2 (BCO2) knockout (KO) and the isogenic background 129S6 (WT) mice. Respiratory supercomplex assembly was examined by blue native PAGE followed by immunoblotting using antibodies against **A**, NDUFB6 of CI and/or I, complex I; **B**, UQCRC2 of CIII and/or III, complex III; **C**, MTCO2 of CIV and/or IV, complex IV. III₂, complex III homodimers; III₂ + IV, supercomplex III₂ + IV; IV₂, complex IV homodimer; Other supercomplexes (SCs), supercomplexes containing CI, CIII, and CIV, the exact number of the I, III, and/or IV in the supercomplex unknown.?, non-identified in the literature. IB, immunoblotting. n=4. **D**, Primary mouse embryonic fibroblasts were stained with MitoSOX (red) and Mito-Tracker (green). MitoSOX and Mito-Tracker signals were quantified using ImageJ. Relative superoxide contents are expressed as MitoSOX/Mito-Tracker. Values are means \pm S.D., n=6 with 2 technical replicates. ** Different from control (WT MEFs), $P < 0.01$. Scale bar, 25 μ m

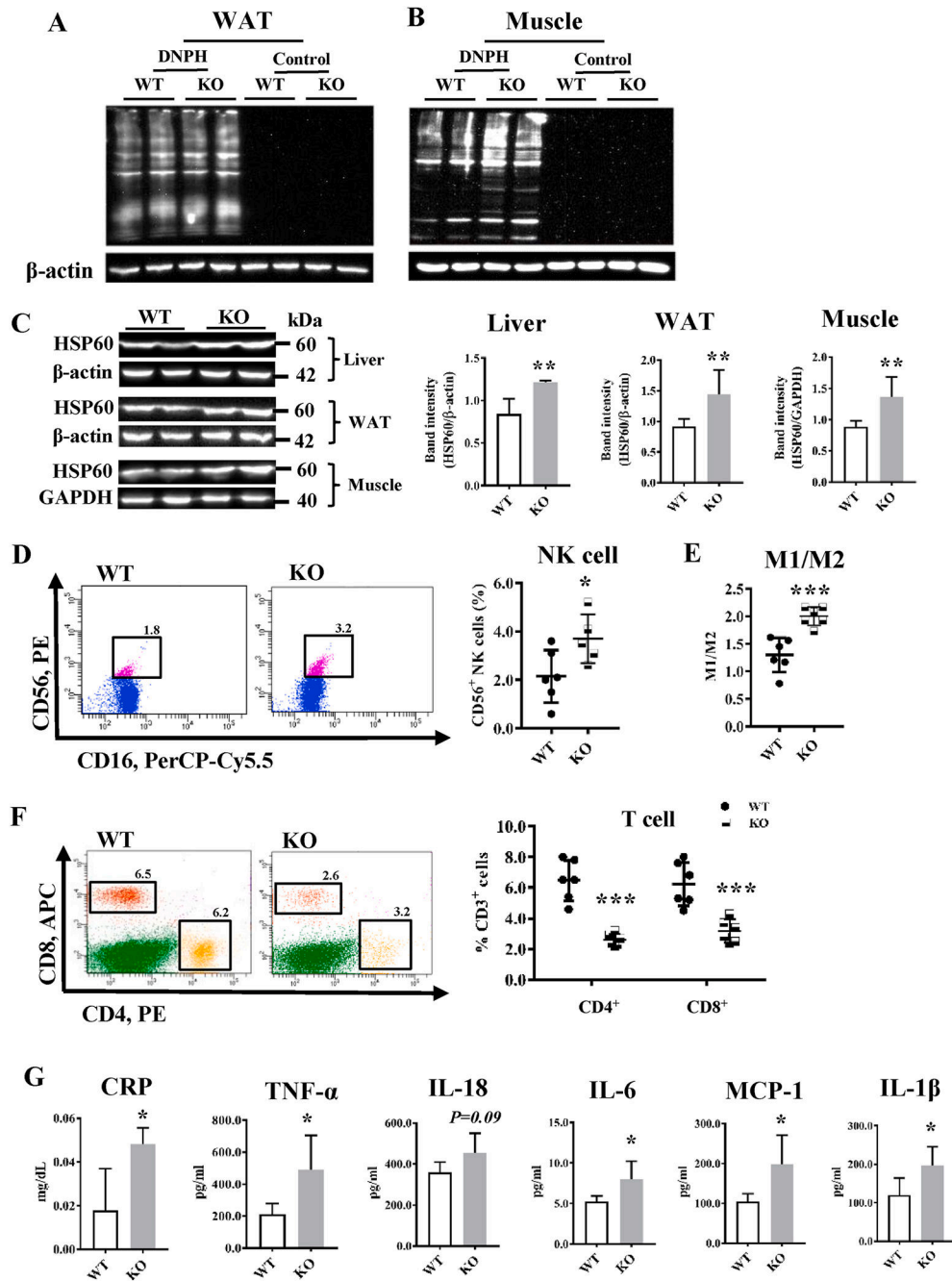


Figure 3. Deficiency of BCO2 leads to oxidative damage and systemic low-grade inflammation
 Plasma, bone marrow, liver, white adipose tissues (WAT), and gastrocnemius muscles (Muscle) were collected from 6-week old male β -carotene oxygenase 2 (BCO2) knockout (KO) and the isogenic background 129S6 (WT) mice. **A-B**, OxyBlot analysis of protein oxidative damage in WAT (**A**) and Muscle (**B**). Left four lanes were DNPH-treated, and the right four lanes were negative controls. **C**, Representative immunoblotting and quantification results of HSP60 in the liver, WAT, and Muscle lysates. **D**, Representative flow cytometry dot plots and quantitative results of NK cells derived from the bone marrow. **E**, The ratio of M1 to M2 macrophages isolated from the bone marrow. **F**, Representative flow cytometry

dot plots and quantitative results of CD4⁺ and CD8⁺ T cells derived from the bone marrow. **G**, Plasma levels of CRP, TNF α , MCP-1, IL-6, IL-1 β , and IL-18. Data were analyzed by Student's *t*-test. Values are means \pm S.D., n=6–8, with 2 technical replicates. * Significant difference from WT, P < 0.05. *P < 0.05; **P < 0.01; ***P < 0.001. CRP, C-reactive protein; HSP60, heat shock protein 60, mitochondrial; IL-1 β , interleukin 1 β ; IL-6, interleukin 6, IL-18, interleukin 18; MCP-1, monocyte chemoattractant protein-1; NK cell, natural killer cell; TNF- α , tumor necrosis factor α .

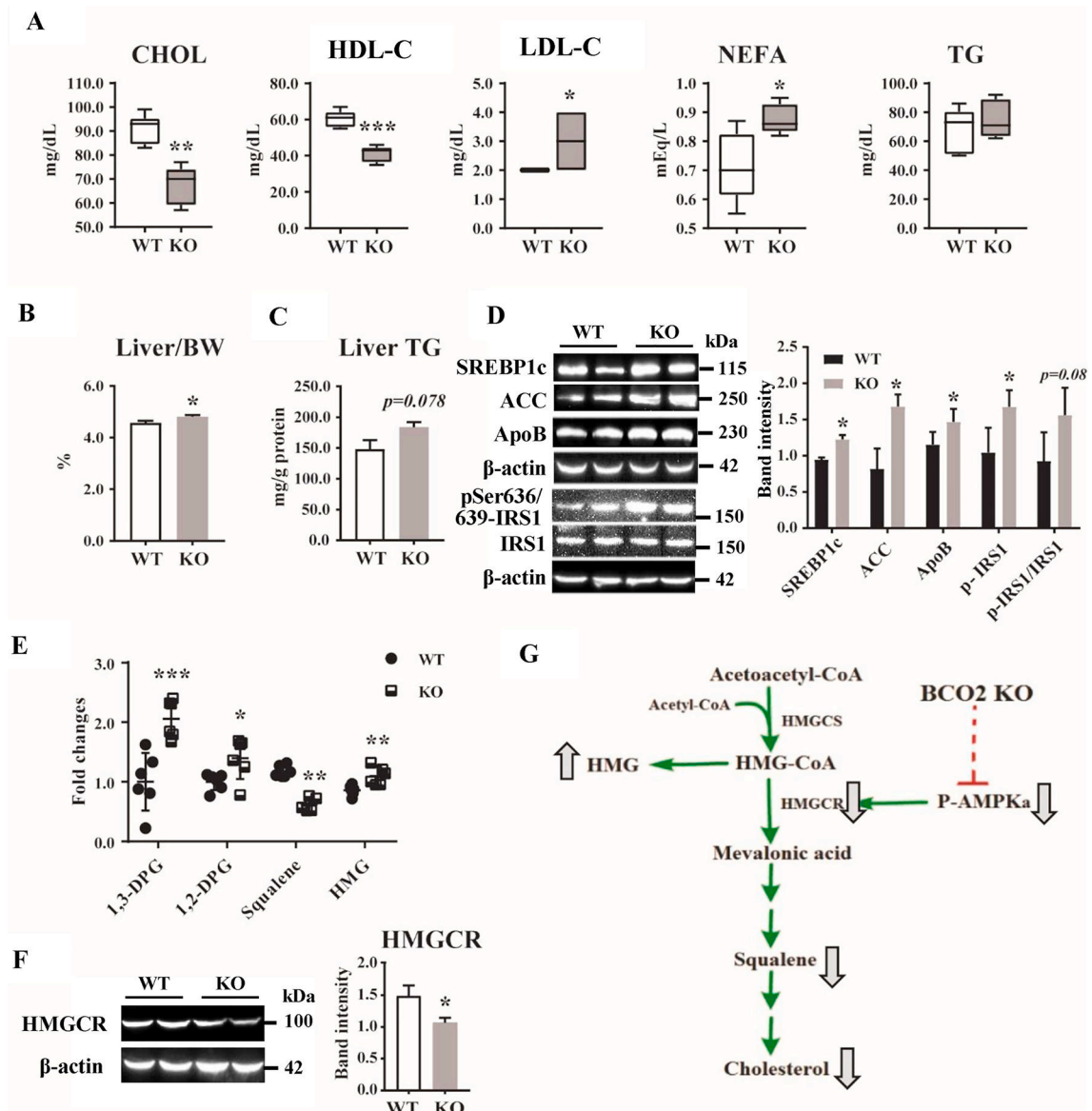


Figure 4. Deficiency of BCO2 is associated with dyslipidemia and impaired lipid metabolism in liver

6-week old male β -carotene oxygenase 2 (BCO2) knockout (KO) and the isogenic background 129S6 (WT) mice were used. **A**, Plasma total cholesterol (CHOL), HDL-C, LDL-C, NEFA, and TG levels. **B**, Percent of liver weight by body weight (BW). **C**, Liver TG content. **D**, Representative immunoblotting and quantification of liver lysate for proteins associated with lipid metabolism. **E**, Contents of hepatic DAG (e.g., 1,3-DPG and 1,2-DPG), HMG, and squalene. **F**, Representative immunoblotting and quantification of HMGCR in liver lysates. **G**, Brief scheme of altered cholesterol synthesis in BCO2 KO mice. Data were analyzed by Student's *t*-test. Values are means \pm S.D., n=6–8 with 2 technical replicates. * Significant difference from WT, $P < 0.05$. * $P < 0.05$; ** $P < 0.01$ *** $p < 0.001$. 1,2-DPG, 1,2-dipalmitoylglycerol; 1,3-DPG, 1,3-dipalmitoylglycerol; ACC, acetyl-CoA carboxylase; AMPK α , AMP-activated protein kinase α ; ApoB, Apolipoprotein B; DAG, diacylglycerol;

HDL-C, high-density lipoprotein cholesterol; HMG, 3-hydroxy-3-methylglutarate; HMGCR, HMG-CoA reductase; HMGCS, HMG-CoA synthase; IRS1, insulin receptor substrate 1; pSer636/639-IRS1, phosphorylation of IRS1 on Ser636/639; LDL-C, low-density lipoprotein cholesterol; NEFA, non-esterified fatty acid; SREBP1c, sterol regulatory element-binding protein 1 c; TG, triglyceride

Author Manuscript

Author Manuscript

Author Manuscript

Author Manuscript

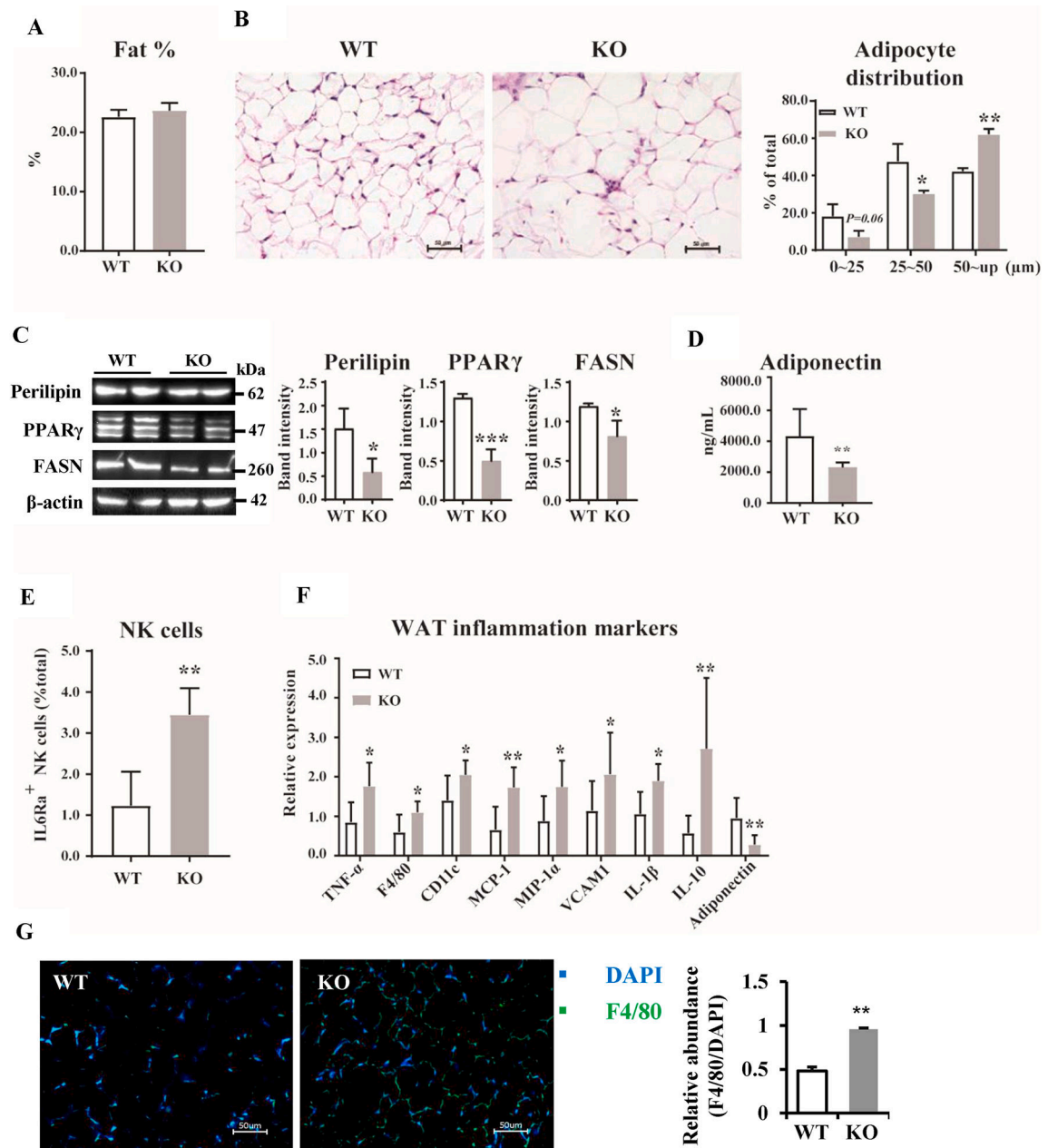


Figure 5. Deficiency of β -carotene oxygenase 2 (BCO2) leads to adipocyte hypertrophy and inflammation in white adipose tissues (WAT) of male mice at 6 weeks of age

A, Total body fat% (n = 6–8). **B**, Representative histology images of WAT depots (2 left panels) and quantification of adipocyte distribution (right) (n = 6–8). Scale bar, 50 μ m. **C**, Representative immunoblotting and quantification of perilipin, PPAR γ , and FASN (n = 6–8). **D**, Plasma adiponectin levels (n = 8–10). **E**, IL6Ra⁺ NK cells in WAT (n = 4–6). **F**, Real-time PCR analyses of genes associated with inflammation in WAT (n = 6–7). **G**, immunohistochemistry of F4/80⁺ cells in WAT. Representative images are shown on the left, with quantification on the right (n = 5). Scale bar, 50 μ m. Values are means \pm S.D., n various with 2 technical replicates. * Significant difference from WT, P < 0.05. **P < 0.05; ***P < 0.01***p < 0.001. CD11c, integrin alpha X; DAPI, 4',6-diamidino-2-phenylindole; F4/80,

F4/80, EGF-like module-containing mucin-like hormone receptor-like 1; FASN, fatty acid synthase; IL-1 β , interleukin 1 β ; IL-10, interleukin 10; MCP-1, monocyte chemoattractant protein-1; MIP-1 α : macrophage inflammatory protein 1 α ; NK cells, natural killer cells; PPAR γ , peroxisome proliferator-activated receptor γ ; WT, wild type mice; TNF- α , tumor necrosis factor α ; VCAM1: vascular cell adhesion protein 1

Author Manuscript

Author Manuscript

Author Manuscript

Author Manuscript

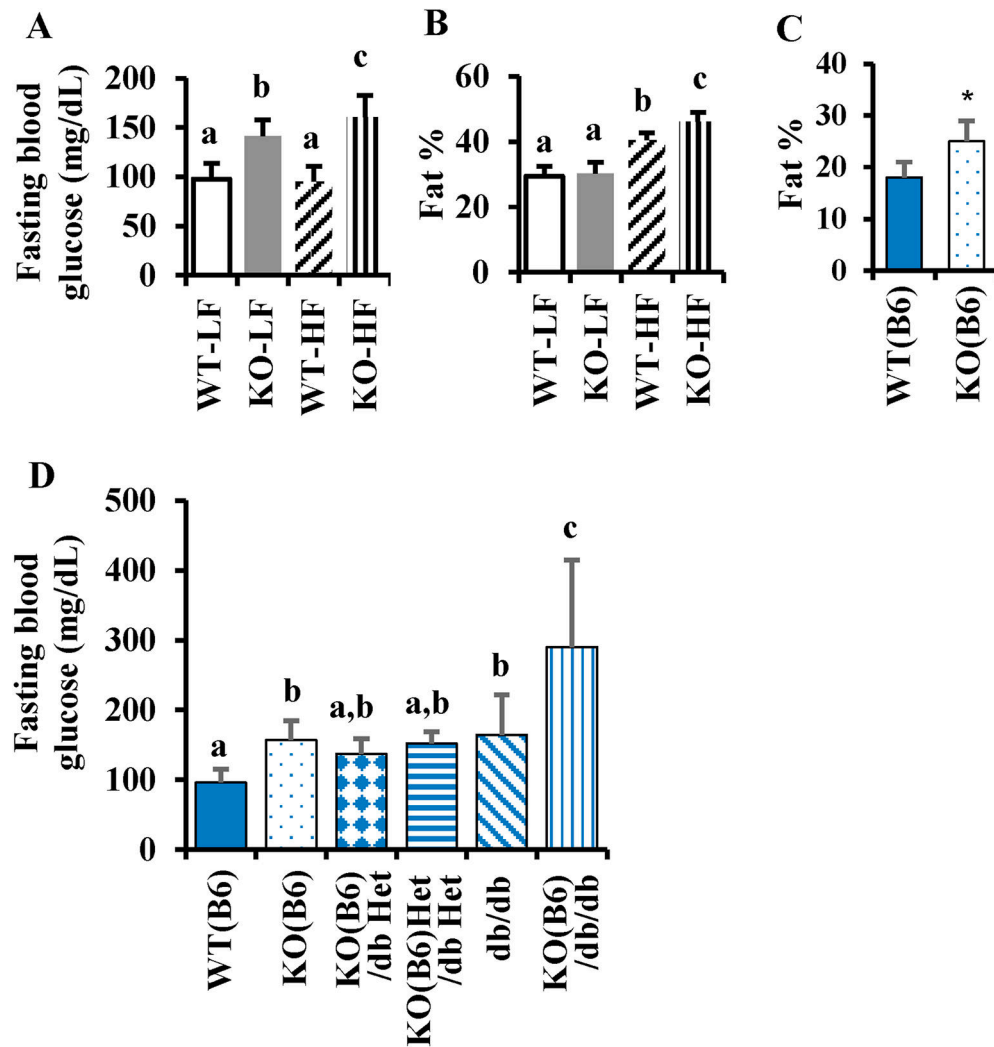


Figure 6. Deficiency of BCO2 increases the susceptibility to high-fat diet-induced obesity and hyperglycemia

Six-week-old male β -carotene oxygenase 2 (BCO2) knockout (KO) and the isogenic background 129S6 (WT) mice were fed low-fat (LF, 10 kCal % fat and 17 kCal % sucrose) or high-fat (HF, 45 kCal % fat and 17 kCal % sucrose) diets for 28 weeks. At the termination of the study, fasting blood glucose (A) and whole-body fat % (B) were measured and shown. Data were analyzed by two-way ANOVA. Values are means \pm S.D., n=12. Labeled means without a common letter differ, $P < 0.05$. Whole-body fat % in 6-week old male β -carotene oxygenase 2 (BCO2) knockout in a C57BL/6J background (KO(B6)) and the isogenic background C57BL/6J (WT(B6)) mice (C). Data were analyzed by Student's t-test. Values are means \pm S.D., n=8. * statistical significance compared to WT(B6), $P < 0.05$. KO(B6) mice were backcrossed with db/db. Male offsprings with BCO2 and leptin receptor depletion (db/db) were subject to the fasting blood glucose test at 4 weeks of age (D). Data were analyzed with one-way ANOVA. Values are means \pm S.D., n=6–8. Labeled means without a common letter differ, $P < 0.05$. db/db, leptin receptor knockout homozygous; db Het, leptin receptor knockout heterozygous; KO-HF, KO fed HF diet; KO-LF, KO fed LF diet; KO(B6), BCO2 knockout homozygous in a C57BL/6J background; KO(B6)/db/db, BCO2 and leptin

receptor double knockout homozygous; KO(B6)Het, BCO2 knockout heterozygous in C57BL/6J background; WT-HF, WT fed HF diet; WT-LF, WT fed LF diet

Author Manuscript

Author Manuscript

Author Manuscript

Author Manuscript

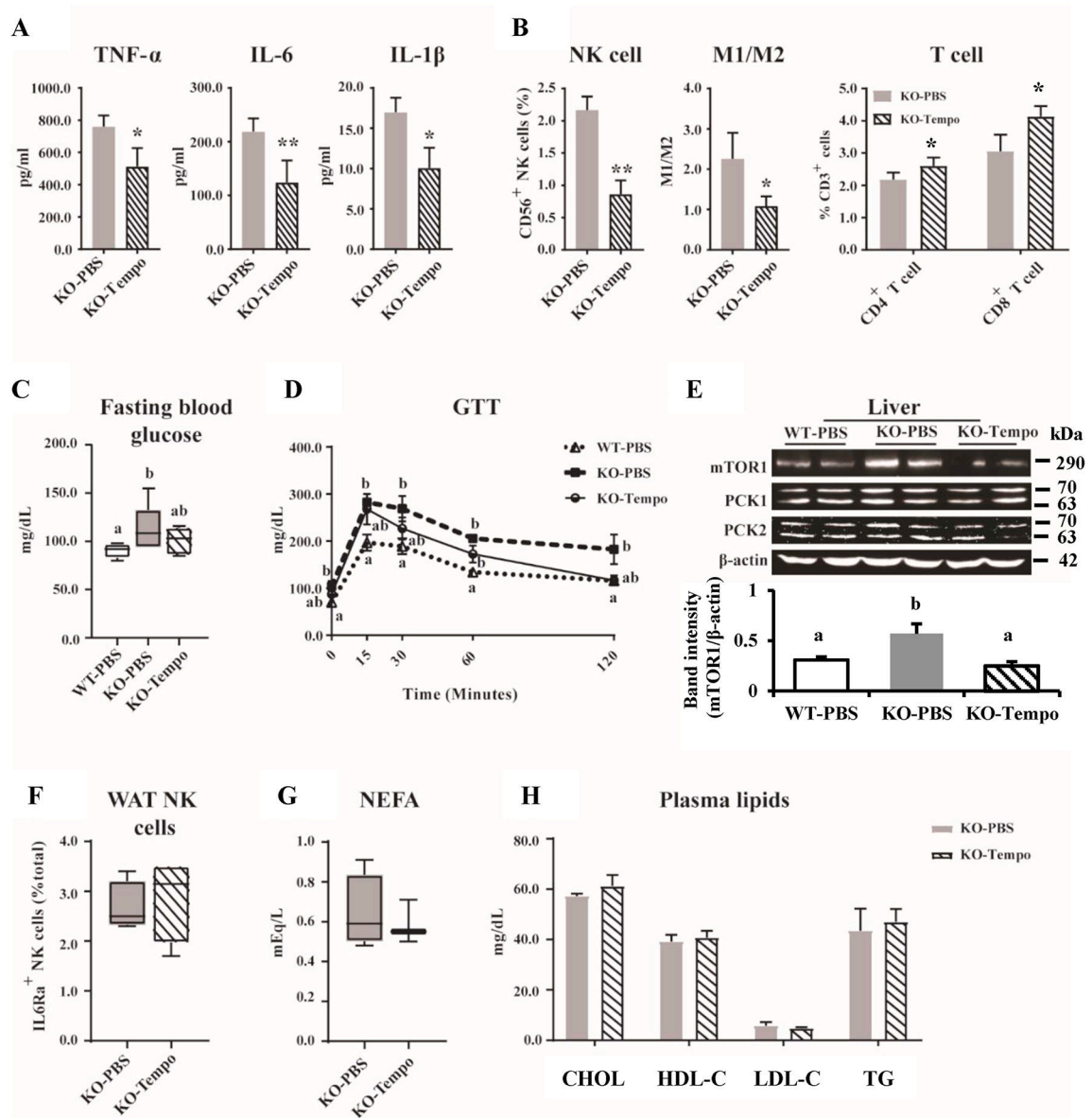


Figure 7. Mito-TEMPO attenuates BCO2 deficiency-induced systemic low-grade inflammation
Six-week-old male KO mice received intraperitoneal (i.p.) injection of Mito-TEMPO (3.5 mg/kg BW/day, KO-Tempo) or sterile PBS (KO-PBS) for 7 consecutive days [32]. Age- and gender-matched WT mice were injected intraperitoneally with sterile PBS as control (WT-PBS). Glucose tolerance test (GTT) was performed in mice on day 6 of the Mito-TEMPO administration. At the termination of the administration, mice were sacrificed for biochemical assessments. **A**, Plasma levels of TNF α , IL-1 β , and IL-6. **B**, Quantification of NK cell, CD4⁺ T cell, CD8⁺ T cell, and the ratio of M1 to M2 macrophages in the bone marrow cells. **C**, Fasting blood glucose. **D**, Glucose tolerance test. **E**, Representative immunoblotting images and quantification of mTOR1, PCK1, and PCK2. **F**, Quantification of IL6Ra⁺ NK cell populations in WAT by flow cytometry. **G**, Plasma NEFA levels. **H**, Plasma levels of CHOL, HDL-C, LDL-C, and TG. Data were analyzed by Student's *t*-test (*

Significant difference from WT, $P < 0.05$. * $P < 0.05$; ** $P < 0.01$ *** $p < 0.001$) or one-way ANOVA (Labeled means without a common letter differ, $P < 0.05$). Values are means \pm S.D., $n=4-8$, with 2 technical replicates. CHOL, cholesterol; HDL-C, high-density lipoprotein cholesterol; IL-1 β , interleukin 1 β ; IL-6, interleukin 6; LDL-C, low-density lipoprotein cholesterol; Mito-TEMPO, (2-(2,2,6,6-Tetramethylpiperidin-1-oxyl-4-ylamino)-2-oxoethyl) triphenyl-phosphonium chloride, monohydrate; mTOR1, mammalian target of rapamycin 1; NEFA, non-esterified fatty acids; NK cells, natural killer cells; PCK1, phosphoenolpyruvate carboxykinase 1; PCK2, phosphoenolpyruvate carboxykinase 2; TG, triglyceride; TNF- α , tumor necrosis factor α ; WAT, white adipose tissues